Published OnlineFirst April 5, 2011; DOI:10.1158/0008-5472.CAN-10-3482

mutation promotes, while Wt-TFAM inhibits cell growth in CRC with MSI.

Mut-TFAM renders CRC cells resistant to cisplatin-induced apoptosis

CRC with MSI exhibits low level of resistance to cisplatin (27, 28). To explore the role of the *TFAM* truncating mutation in cisplatin resistance of CRC with MSI, we treated Lenti-Wt-TFAM- or Lenti-vector-infected RKO cells with cisplatin and followed by apoptosis analysis using flow cytometry. The RKO cells expressing Wt-TFAM were more susceptible to cisplatin-induced apoptosis, as indicated by an up to 8-fold increase in sub-G_1 stage cells (Fig. 4A) and an up to 4-fold increase in cytochrome *c* (Cyt *c*) levels before or after cisplatin treatment (Fig. 4B). In agreement with the Cyt *c* data, the levels of cleaved Parp-1 and Casp 3 were also increased (Fig. 4B). Since Cyt *b* is a mitochondrial gene encoded protein and plays an important role in apoptosis (29), we further examined Cyt *b* levels in those RKO cells. We found that the cytosolic levels of Cyt *b* and cleaved Cyt *b* were higher, while the mitochondrial level of Cyt *b* was lower, in RKO cells infected with Wt-TFAM than in those infected with the control vector (Fig. 4C). These results suggest that CRC cells harboring the *TFAM* frameshift mutation are more resistant to cisplatin through a Cyt *b*-dependent apoptotic mechanism and that the resistance to cisplatin-induced apoptosis in CRC cells with MSI is probably due to the presence of a *TFAM* truncating mutation.

Mut-TFAM downregulates Cyt *b* transcription in CRC with MSI

To understand the mechanism of Mut-TFAM in the regulation of Cyt *b*, we assessed the expression levels of *CYTB* and *ND1* in RKO cells expressing Wt-TFAM. The transcriptional levels of both *ND1* and *CYTB* were elevated significantly (Fig. 5A, $P < 0.05$). The protein levels of both ND1 and Cyt *b* were also elevated (Fig. 5B). Since *CYTB* is a mitochondrial gene and TFAM regulates transcription of mitochondrial genes by binding to the HSP (30), we further tested our hypothesis that Mut-TFAM might impair the transcriptional regulation of *CYTB* by aberrant interaction with HSP in CRC with MSI. The interaction assay of equivalent amounts of GST-Wt-TFAM or GST-Mut-TFAM synthesized in *E. coli* with the HSP revealed that the relative binding ability of Wt-TFAM was significantly higher than that of Mut-TFAM (Fig. 5C and D, $P < 0.01$). Moreover, we found that more Mut-TFAM was present in the NP40-soluble fraction than Wt-TFAM, while more Wt-TFAM was in the pellet fraction, where most of the mtDNA was contained (Fig. 5E). Together, these data suggest that CRC carrying *TFAM* truncating mutation may increase resistance to cisplatin-induced apoptosis through reduced interaction with HSP and downregulation of *CYTB* transcription.

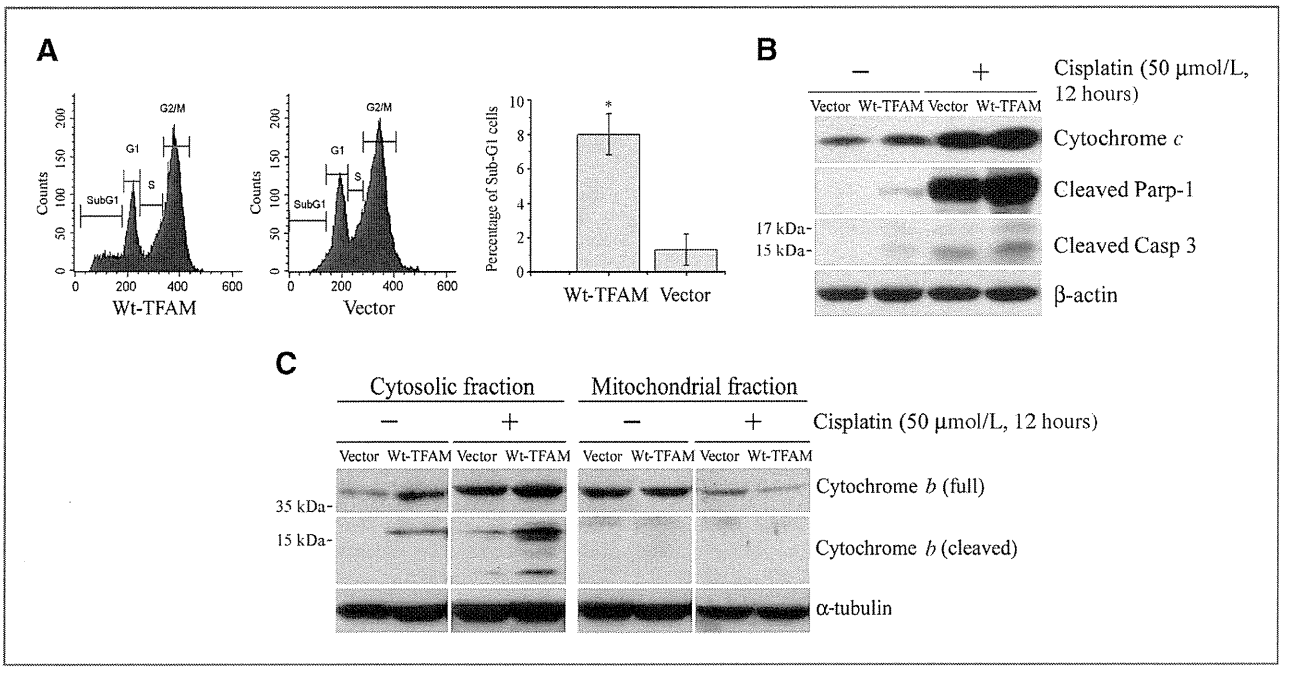

Figure 4. Mutant TFAM confers resistance to cisplatin-induced apoptosis in microsatellite-unstable RKO cells. A, representative flow cytometry images for apoptosis analysis. Cisplatin induced more apoptosis (sub-G1 population) in RKO cells expressing Wt-TFAM (left) than vector control (middle). The proportion of sub-G_1 cells was increased by almost 8-fold (right, $P < 0.05$). Values represent mean ± SE of 3 independent experiments in triplicate. B, Western blots of RKO cell homogenates. The levels of Cyt *c*, cleaved Parp-1 and Casp-3 were higher in Wt-TFAM-expressing RKO cells and were enhanced by cisplatin treatment compared with vector-expressing RKO cells. C, Western blots showing Wt-TFAM overexpression promoted Cyt *b* release from mitochondria into cytoplasm of RKO cells under the same conditions as in (B). The release was enhanced by cisplatin treatment.

Published OnlineFirst April 5, 2011; DOI:10.1158/0008-5472.CAN-10-3482

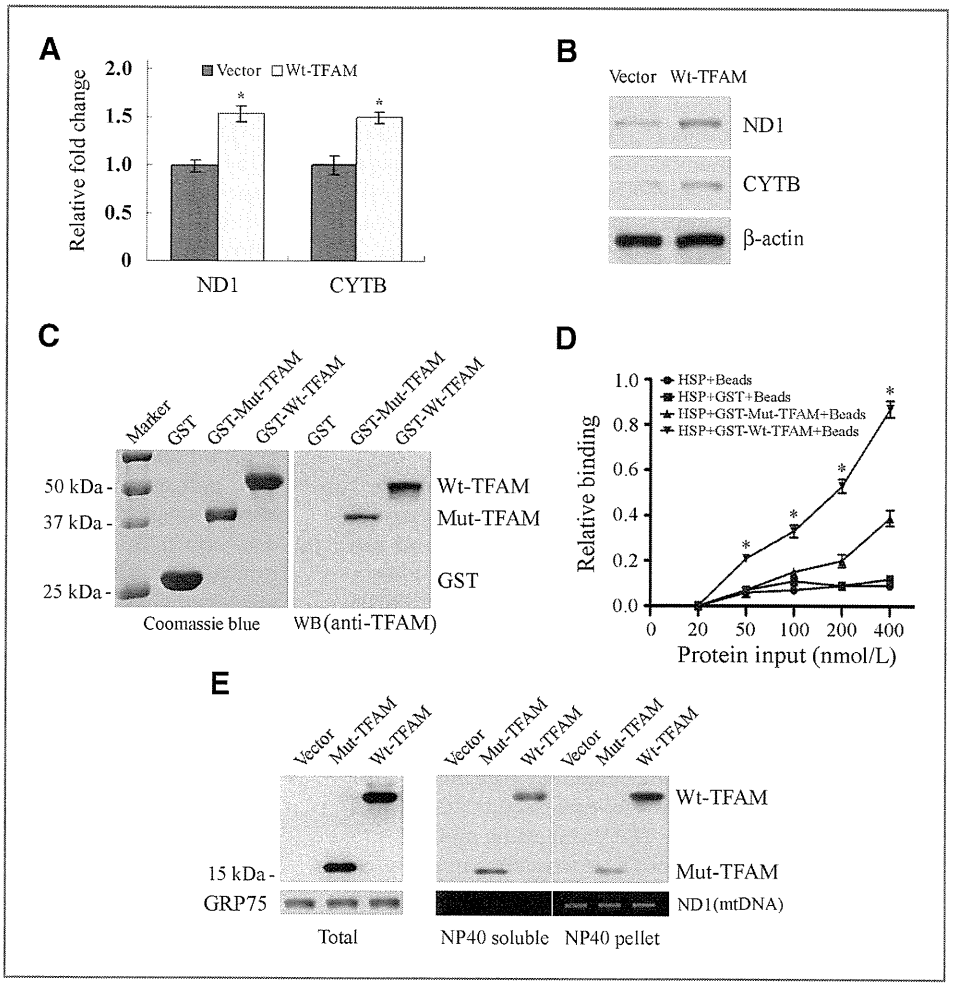

Figure 5. Aberrant regulation of *CYTB* transcription by Mut-TFAM in CRC with MSI. A, qRT-PCR analysis of *ND1* and *CYTB* mRNA in RKO cells expressing Wt-TFAM or vector. Values represent mean ± SD of 3 analyses, $P < 0.05$ for both. B, Western blots showing ND1 and CYTB protein levels in RKO cells as in (A). C, purified GST-Wt-TFAM and GST-Mut-TFAM fusion proteins were visualized by Coomassie blue staining (left) and Western blot with anti-TFAM antibody (right). D, relative binding ability of Wt-TFAM or Mut-TFAM to mitochondrial HSP. Data represent mean ± SE of 3 independent experiments in triplicate, $P < 0.01$. E, distribution of Wt-TFAM and Mut-TFAM in the NP40-soluble or -insoluble fraction of mitochondrial extracts from RKO cells expressing control vector, Wt- or Mut-TFAM. GRP75 was a loading control for mitochondrial protein; *ND1* was PCR-amplified to serve as a mtDNA loading control.

Discussion

The mtDNA depletion or mitochondrial instability is a common event in human cancer, including CRC (31, 32). However, the cause of mtDNA depletion in tumorigenesis is currently unknown. In this study, we provided evidence that mutation in *TFAM*, an important component of the mitochondrial transcription and replication machinery, plays an important role in maintaining mitochondrial stability in CRC. The mtDNA copy number difference between CRC with or without MSI is so striking that low mtDNA copy number might be a potential genetic marker of CRC with MSI, once the current data are validated in a future large cohort analysis. Besides CRC, we also observed mtDNA depletion in non-CRC cell lines with *TFAM* mutations. However, the range of copy numbers in non-CRC cell lines without *TFAM* mutations was wider. Two breast cancer cell lines (MCF-7 and MDA-MB231) without *TFAM* mutations seemed to have low mtDNA copy numbers, similar to those in MSI cell lines with *TFAM* mutations (Fig. 3A, right). But the exact reason remains unknown and needs to be determined. Recently, more genes responsible for maintaining mtDNA stability have been identified, including *TIM17* and *OXA1* (33). It is possible that loss function mutations or epigenetic regulation of *TFAM*, *TIM17*, and *OXA1* may induce mtDNA instability in these non-CRC cells without MSI.

CRC cells with MSI are prone to mutation throughout the genome. It thus presents a significant challenge to determine whether a truncating mutation induced by DNA mismatch repair deficiency functions as a "Driver" to facilitate tumorigenesis or just as a "Bystander". By comparing our data to the 5-point criteria for a *bona fide* target gene from bystander mutations proposed by the NCI group, we found that the *TFAM* truncating mutations fulfill 4 of the 5 criteria: (i) the frequency of the *TFAM* mutation in CRC with MSI is over 75%, way above that of the background; (ii) mut-TFAM promotes cell proliferation, suggesting a functional importance in tumorigenesis; (iii) TFAM interacts with p53 and although the role of TFAM in the p53 pathway is not defined, the p53 pathway genes are commonly mutated in CRC (34, 35); and (iv) biallelic inactivation is not applicable since loss of both *TFAM* alleles has been reported to be embryonic lethal in mouse and results in loss of all mitochondria and apoptosis *in vivo* (11, 36). We noted the prevalence of a 1-base or 2-base deletion detected in these samples. But when 95 subclones of PCR

Published OnlineFirst April 5, 2011; DOI:10.1158/0008-5472.CAN-10-3482

products amplified from a CRC tumor DNA with MSI were sequenced, we did detect low frequencies of 1-base insertion mutations (3.2%; data not shown). The presence of the low frequency of 1-base insertion in the tumor specimen harboring 1-base deletion mutation is probably due to the nature of mitochondrial heteroplasmy (37). Moreover, we did not detect any meaningful *TFAM* mutations in CRC cell lines and tumor specimens without MSI, except for some function-unknown SNPs (data not shown). The absence of *TFAM* mutations in MSS CRC could be due to the small sample size of the current study or the higher frequency of *p53* mutations in MSS CRC than in CRC with MSI (38). It is, therefore, very likely that during mutation selection, only TFAM haploinsufficient cells are selected for tumor growth and the haploinsufficient *TFAM* truncating mutation becomes a predominant one during cancer progression.

Overexpression of Mut-TFAM in promoting cell growth is evident in both RKO and HCT116 cells by our *in vitro* cell proliferation assays. In contrast, Wt-TFAM suppressed cell growth in these 2 cell lines and *in vivo* xenograft tumor growth assays. Intriguingly, overexpression of Mut-TFAM in HEK293 cells induced apoptosis instead of cell growth (data not shown). This is not surprising since *Tfam* knockout mouse displayed massive apoptosis at embryonic day 9.5 and increased apoptosis was observed in the heart of the tissue-specific *Tfam* knockouts (39). These data suggest that the involvement of TFAM in apoptosis is probably temporally regulated and/or may be tissue specific. It will be necessary to find CRC cell lines with MSI, which do not carry *TFAM* truncating mutations to test whether overexpression of *TFAM* truncating mutation or knockdown of *TFAM* in these cells induces apoptosis. Although the detailed mechanism by which Mut-TFAM promotes tumor cell growth remains to be elucidated, our data indicate that loss of the ability to induce Cyt *b* expression and thus the inability to induce Cyt *b*-dependent apoptosis is probably one of the mechanisms for Mut-*TFAM* to induce tumor progression in most microsatellite-unstable CRC.

Accumulating evidence has indicated that the MMR protein is critical for cisplatin-dependent apoptosis in many cancer cells, including CRC, but how loss of MMR protein increases resistance to cisplatin-dependent apoptosis remains unclear (27, 40, 41). The results in our study demonstrated that CRC cells carrying *TFAM* truncating mutations were more resistant to cisplatin-induced apoptosis than were the same cells overexpressing Wt-TFAM. These data thus provide evidence that TFAM is required for the induction of cisplatin-dependent apoptosis in CRC with MSI. It is critical to initiate an investigation of the responsiveness of CRC patients who carry or do not carry *TFAM* truncating mutations to cisplatin-based chemotherapy. Such data may help to improve therapeutic intervention protocols for patients with or without *TFAM* truncating mutations.

In summary, we have shown the presence of high frequency of *TFAM* truncating mutations in human microsatellite-unstable CRC cell lines and primary tumors. The CRC with MSI harboring the *TFAM* truncating mutation displayed impaired mitochondrial stability, dysregulated cell proliferation, mitigated Cyt *b*-dependent apoptosis, and enhanced cisplatin-dependent apoptotic resistance. Our preliminary data also indicate a potential mechanism by which *TFAM* truncating mutation is involved in apoptosis through down-regulation of Cyt *b* transcription due to reduced interaction with mitochondrial HSP. These findings support the role of TFAM and mitochondrial stability in CRC tumorigenesis. This may have potential relevance in the pharmacogenetic selection of CRC patients for treatment with cisplatin or other drugs.

Disclosure of Potential Conflicts of Interest

No potential conflicts of interest were disclosed.

Acknowledgments

The authors would like to thank Dr. Jay K. Kolls and Dr. Matthew K. Gilbert for their critical review and revising this manuscript. This project was supported by Cancer Research Fund from Louisiana Cancer Research Consortium (LCRC) to W. Liu.

The costs of publication of this article were defrayed in part by the payment of page charges. This article must therefore be hereby marked *advertisement* in accordance with 18 U.S.C. Section 1734 solely to indicate this fact.

Received September 24, 2010; revised February 7, 2011; accepted February 11, 2011; published OnlineFirst April 5, 2011.

References

1. Lengauer C, Kinzler KW, Vogelstein B. DNA methylation and genetic instability in colorectal cancer cells. Proc Natl Acad Sci U S A 1997;94:2545–50.
2. Bronner CE, Baker SM, Morrison PT, Warren G, Smith LG, Lescoe MK, et al. Mutation in the DNA mismatch repair gene homologue hMLH1 is associated with hereditary non-polyposis colon cancer. Nature 1994;368:258–61.
3. Thibodeau SN, Bren G, Schaid D. Microsatellite instability in cancer of the proximal colon. Science 1993;260:816–9.
4. Boland CR, Thibodeau SN, Hamilton SR, Sidransky D, Eshleman JR, Burt RW, et al. A National Cancer Institute Workshop on Microsatellite Instability for cancer detection and familial predisposition: development of international criteria for the determination of microsatellite instability in colorectal cancer. Cancer Res 1998;58:5248–57.
5. Duval A, Hamelin R. Mutations at coding repeat sequences in mismatch repair-deficient human cancers: toward a new concept of target genes for instability. Cancer Res 2002;62:2447–54.
6. Liu W, Dong X, Mai M, Seelan RS, Taniguchi K, Krishnadath KK, et al. Mutations in AXIN2 cause colorectal cancer with defective mismatch repair by activating beta-catenin/TCF signalling. Nat Genet 2000;26:146–7.
7. Markowitz S, Wang J, Myeroff L, Parsons R, Sun L, Lutterbaugh J, et al. Inactivation of the type II TGF-beta receptor in colon cancer cells with microsatellite instability. Science 1995;268:1336–8.
8. Rampino N, Yamamoto H, Ionov Y, Li Y, Sawai H, Reed JC, et al. Somatic frameshift mutations in the BAX gene in colon cancers of the microsatellite mutator phenotype. Science 1997;275:967–9.
9. Ropero S, Fraga MF, Ballestar E, Hamelin R, Yamamoto H, Boix-Chornet M, et al. A truncating mutation of HDAC2 in human cancers confers resistance to histone deacetylase inhibition. Nat Genet 2006;38:566–9.
10. Kang D, Kim SH, Hamasaki N. Mitochondrial transcription factor A (TFAM): roles in maintenance of mtDNA and cellular functions. Mitochondrion 2007;7:39–44.

Published OnlineFirst April 5, 2011; DOI:10.1158/0008-5472.CAN-10-3482

11. Larsson NG, Wang J, Wilhelmsson H, Oldfors A, Rustin P, Lewandoski M, et al. Mitochondrial transcription factor A is necessary for mtDNA maintenance and embryogenesis in mice. Nat Genet 1998;18:231–6.
12. Ekstrand MI, Falkenberg M, Rantanen A, Park CB, Gaspari M, Hultenby K, et al. Mitochondrial transcription factor A regulates mtDNA copy number in mammals. Hum Mol Genet 2004;13:935–44.
13. Bender A, Krishnan KJ, Morris CM, Taylor GA, Reeve AK, Perry RH, et al. High levels of mitochondrial DNA deletions in substantia nigra neurons in aging and Parkinson disease. Nat Genet 2006;38:515–7.
14. Hansson A, Hance N, Dufour E, Rantanen A, Hultenby K, Clayton DA, et al. A switch in metabolism precedes increased mitochondrial biogenesis in respiratory chain-deficient mouse hearts. Proc Natl Acad Sci U S A 2004;101:3136–41.
15. Ekstrand MI, Terzioglu M, Galter D, Zhu S, Hofstetter C, Lindqvist E, et al. Progressive parkinsonism in mice with respiratory-chain-deficient dopamine neurons. Proc Natl Acad Sci U S A 2007;104:1325–30.
16. Bertram L, McQueen MB, Mullin K, Blacker D, Tanzi RE. Systematic meta-analyses of Alzheimer disease genetic association studies: the AlzGene database. Nat Genet 2007;39:17–23.
17. Guo J, Cagatay T, Zhou G, Chan CC, Blythe S, Suyama K, et al. Mutations in the human naked cuticle homolog NKD1 found in colorectal cancer alter Wnt/Dvl/beta-catenin signaling. PLoS One 2009;4:e7982.
18. Liu W, Smith DI, Rechtzigel KJ, Thibodeau SN, James CD. Denaturing high performance liquid chromatography (DHPLC) used in the detection of germline and somatic mutations. Nucleic Acids Res 1998;26:1396–400.
19. Goldstein JC, Waterhouse NJ, Juin P, Evan GI, Green DR. The coordinate release of cytochrome *c* during apoptosis is rapid, complete and kinetically invariant. Nat Cell Biol 2000;2:156–62.
20. Ohno T, Umeda S, Hamasaki N, Kang D. Binding of human mitochondrial transcription factor A, an HMG box protein, to a four-way DNA junction. Biochem Biophys Res Commun 2000;271:492–8.
21. Liu CS, Tsai CS, Kuo CL, Chen HW, Lii CK, Ma YS, et al. Oxidative stress-related alteration of the copy number of mitochondrial DNA in human leukocytes. Free Radic Res 2003;37:1307–17.
22. Livak KJ, Schmittgen TD. Analysis of relative gene expression data using real-time quantitative PCR and the 2(-delta delta C(T)) method. Methods 2001;25:402–8.
23. Ohgaki K, Kanki T, Fukuoh A, Kurisaki H, Aoki Y, Ikeuchi M, et al. The C-terminal tail of mitochondrial transcription factor a markedly strengthens its general binding to DNA. J Biochem 2007;141:201–11.
24. Fukuoh A, Kang D. Methods for assessing binding of mitochondrial transcription factor A (TFAM) to DNA. Methods Mol Biol 2009;554:87–101.
25. Williams CD, Linch DC, Watts MJ, Thomas NS. Characterization of cell cycle status and E2F complexes in mobilized CD34+ cells before and after cytokine stimulation. Blood 1997;90:194–203.
26. Kanki T, Ohgaki K, Gaspari M, Gustafsson CM, Fukuoh A, Sasaki N, et al. Architectural role of mitochondrial transcription factor A in maintenance of human mitochondrial DNA. Mol Cell Biol 2004;24:9823–34.
27. Fink D, Aebi S, Howell SB. The role of DNA mismatch repair in drug resistance. Clin Cancer Res 1998;4:1–6.
28. Honecker F, Wermann H, Mayer F, Gillis AJ, Stoop H, van Gurp RJ, et al. Microsatellite instability, mismatch repair deficiency, and BRAF mutation in treatment-resistant germ cell tumors. J Clin Oncol 2009;27:2129–36.
29. Komarov AP, Rokhlin OW, Yu CA, Gudkov AV. Functional genetic screening reveals the role of mitochondrial cytochrome *b* as a mediator of FAS-induced apoptosis. Proc Natl Acad Sci U S A 2008;105:14453–8.
30. Ikeda S, Sumiyoshi H, Oda T. DNA binding properties of recombinant human mitochondrial transcription factor 1. Cell Mol Biol (Noisy-le-grand) 1994;40:489–93.
31. Lee HC, Yin PH, Lin JC, Wu CC, Chen CY, Wu CW, et al. Mitochondrial genome instability and mtDNA depletion in human cancers. Ann N Y Acad Sci 2005;1042:109–22.
32. Lu J, Sharma LK, Bai Y. Implications of mitochondrial DNA mutations and mitochondrial dysfunction in tumorigenesis. Cell Res 2009;19:802–15.
33. Iacovino M, Granycome C, Sembongi H, Bokori-Brown M, Butow RA, Holt IJ, et al. The conserved translocase Tim17 prevents mitochondrial DNA loss. Hum Mol Genet 2009;18:65–74.
34. Yoshida Y, Izumi H, Torigoe T, Ishiguchi H, Itoh H, Kang D, et al. P53 physically interacts with mitochondrial transcription factor A and differentially regulates binding to damaged DNA. Cancer Res 2003;63:3729–34.
35. Wong TS, Rajagopalan S, Freund SM, Rutherford TJ, Andreeva A, Townsley FM, et al. Biophysical characterizations of human mitochondrial transcription factor A and its binding to tumor suppressor p53. Nucleic Acids Res 2009;37:6765–83.
36. Wang J, Silva JP, Gustafsson CM, Rustin P, Larsson NG. Increased in vivo apoptosis in cells lacking mitochondrial DNA gene expression. Proc Natl Acad Sci U S A 2001;98:4038–43.
37. Chatterjee A, Mambo E, Sidransky D. Mitochondrial DNA mutations in human cancer. Oncogene 2006;25:4663–74.
38. Samowitz WS, Holden JA, Curtin K, Edwards SL, Walker AR, Lin HA, et al. Inverse relationship between microsatellite instability and K-ras and p53 gene alterations in colon cancer. Am J Pathol 2001;158:1517–24.
39. Li H, Wang J, Wilhelmsson H, Hansson A, Thoren P, Duffy J, et al. Genetic modification of survival in tissue-specific knockout mice with mitochondrial cardiomyopathy. Proc Natl Acad Sci U S A 2000;97:3467–72.
40. Martin LP, Hamilton TC, Schilder RJ. Platinum resistance: the role of DNA repair pathways. Clin Cancer Res 2008;14:1291–5.
41. Topping RP, Wilkinson JC, Scarpinato KD. Mismatch repair protein deficiency compromises cisplatin-induced apoptotic signaling. J Biol Chem 2009;284:14029–39.

Phosphorylation of Serine 114 on Atg32 mediates mitophagy

Yoshimasa Aoki, Tomotake Kanki, Yuko Hirota, Yusuke Kurihara, Tetsu Saigusa, Takeshi Uchiumi, and Dongchon Kang
Department of Clinical Chemistry and Laboratory Medicine, Kyushu University Graduate School of Medical Sciences, Fukuoka 812-8582, Japan

ABSTRACT **Mitophagy, which selectively degrades mitochondria via autophagy, has a significant role in mitochondrial quality control. When mitophagy is induced in yeast, mitochondrial residential protein Atg32 binds Atg11, an adaptor protein for selective types of autophagy, and it is recruited into the vacuole along with mitochondria. The Atg11–Atg32 interaction is believed to be the initial molecular step in which the autophagic machinery recognizes mitochondria as a cargo, although how this interaction is mediated is poorly understood. Therefore, we studied the Atg11–Atg32 interaction in detail. We found that the C-terminus region of Atg11, which included the fourth coiled-coil domain, interacted with the N-terminus region of Atg32 (residues 100–120). When mitophagy was induced, Ser-114 and Ser-119 on Atg32 were phosphorylated, and then the phosphorylation of Atg32, especially phosphorylation of Ser-114 on Atg32, mediated the Atg11–Atg32 interaction and mitophagy. These findings suggest that cells can regulate the amount of mitochondria, or select specific mitochondria (damaged or aged) that are degraded by mitophagy, by controlling the activity and/or localization of the kinase that phosphorylates Atg32. We also found that Hog1 and Pbs2, which are involved in the osmoregulatory signal transduction cascade, are related to Atg32 phosphorylation and mitophagy.**

Monitoring Editor
Suresh Subramani
University of California, San Diego

Received: Feb 18, 2011
Revised: Jun 30, 2011
Accepted: Jul 5, 2011

INTRODUCTION

The mitochondrion is an organelle that produces energy through the use of an electron transport chain and oxidative phosphorylation. On the other hand, mitochondria are the major source of cellular reactive oxygen species (ROS), which cause oxidative damage to mitochondrial DNA, protein, and lipids, and the accumulation of this damage is related to many disorders, such as neurodegenerative diseases, diabetes mellitus, cancer, and aging (Wallace, 2005). Accordingly, appropriate quality control of mitochondria is important to maintain proper cellular homeostasis. Mitochondria have several maintenance systems, including a protein degradation system (Rep and Grivell, 1996; Friguet *et al.*, 2008; Voos, 2009), DNA repair enzymes (Larsson and Clayton, 1995; Bogenhagen, 1999), and phospholipid hydroperoxide glutathione peroxidase (Arai *et al.*, 1999). In addition to these mitochondrial maintenance systems, recent studies from yeast to mammals suggest that mitochondria autophagy (mitophagy) is one of the primary systems that maintains mitochondrial quality by eliminating dysfunctional mitochondria (Elmore *et al.*, 2001; Rodriguez-Enriquez *et al.*, 2004; Priault *et al.*, 2005; Nowikovsky *et al.*, 2007; Narendra *et al.*, 2008; Narendra and Youle, 2011; Twig *et al.*, 2008), although the molecular process of mitophagy is still poorly understood.

Macroautophagy (bulk autophagy) is a nonspecific degradation process of cytoplasmic components that is highly conserved among eukaryotes. After certain cellular stresses, such as nutrient starvation, cytosolic double-membrane vesicles emerge and sequester cytoplasmic proteins and organelles as cargoes, and then the vesicles deliver those cargoes into the lysosome/vacuole (Nakatogawa *et al.*, 2009; Yang and Klionsky,

This article was published online ahead of print in MBoC in Press (http://www.molbiolcell.org/cgi/doi/10.1091/mbc.E11-02-0145) on July 14, 2011.

Address correspondence to: Tomotake Kanki (kanki@cclm.med.kyushu-u.ac.jp).

Abbreviations used: Ape1, aminopeptidase I; Cvt, cytoplasm-to-vacuole targeting; GFP, green fluorescent protein; MAPK, mitogen-activated protein kinase; MAPKK, mitogen-activated protein kinase kinase; PA, protein A; PAS, preautophagosomal structure/phagophore assembly site; ROS, reactive oxygen species.

2010). In contrast to macroautophagy, selective autophagy targets a specific cellular component as a cargo (Johansen and Lamark, 2011). Selective autophagy in yeast includes the cytoplasm-to-vacuole targeting (Cvt) pathway, pexophagy, and mitophagy. The Cvt pathway is an autophagy-like process that delivers the Cvt complex (aminopeptidase I [Ape1] and α-mannosidase complex) and Ape4 from the cytoplasm to vacuoles without delivering any additional known cargo to the vacuoles (Klionsky and Emr, 2000; Yorimitsu and Klionsky, 2005; Yuga *et al.*, 2011), whereas pexophagy and mitophagy are the selective degradation of peroxisomes and mitochondria, respectively, via autophagy (Lemasters, 2005; Oku and Sakai, 2010). Studies on *Saccharomyces cerevisiae* and other fungi have identified 35 autophagy-related (*ATG*) genes. Most of the *ATG* genes are required for both macroautophagy and selective autophagy, whereas some *ATG* genes, such as *ATG11*, *ATG19*, *Pichia pastoris ATG30* (*Pp*ATG30), and *ATG32*, play a role only in selective autophagy. Atg19 is a receptor protein for the Cvt pathway, which binds the Cvt complex and then interacts with Atg11, an adaptor protein for selective autophagy. Atg11 recruits the Cvt complex to the preautophagosomal structure/phagophore assembly site (PAS), where sequestering cytosolic vesicles are generated (Shintani *et al.*, 2002). PpAtg30 is also a receptor protein for pexophagy, which localizes to peroxisomes, and is bound by PpAtg11, allowing recruitment of the peroxisomes to the PAS (Farre *et al.*, 2008). Similarly, during mitophagy, Atg11 interacts with the mitochondrial residential receptor Atg32 and recruits mitochondria to the PAS (Kanki *et al.*, 2009c; Okamoto *et al.*, 2009b). Thus, selective autophagy strictly recognizes and degrades the cargo through the cargo-specific receptor and Atg11 interaction. However, it is poorly understood how the receptor–Atg11 interaction, especially the Atg32–Atg11 interaction, is regulated.

Recent studies in mammals revealed that mitophagy is inevitably involved in cellular physiology and disease. For example, during erythroid cell maturation, mitochondria are eliminated by mitochondrial outer membrane protein Nix-related mitophagy (Schweers *et al.*, 2007; Sandoval *et al.*, 2008). Similarly, during adipose tissue differentiation, mitochondria are eliminated by autophagy (Goldman *et al.*, 2010). Loss-of-function mutations of the *PARK2* and *PARK6* genes, which encode Parkin and PINK1, respectively, cause early-onset Parkinson disease. PINK1 can stably localize on the outer membrane of the impaired mitochondria and recruit Parkin from the cytosol to the mitochondria. Parkin accumulated on mitochondria ubiquitinates mitochondrial proteins and induces mitophagy to degrade impaired mitochondria (Narendra *et al.*, 2008, 2010; Narendra and Youle, 2011). Despite the important role of mitophagy in cellular physiology and disease, the molecular mechanism and regulation of mitophagy are unknown.

To determine the molecular mechanism and the regulation of mitophagy, we studied the Atg11–Atg32 interaction in detail. We found that the C-terminus region of Atg11, which includes the fourth coiled-coil domain of the protein, interacts with the N-terminus region, especially residues of 100–120, of Atg32. We further found that when mitophagy is induced, Ser-114 and Ser-119 on Atg32 are phosphorylated by Ser/Thr protein kinase. The phosphorylation of Atg32, especially phosphorylation of Ser-114 on Atg32, is required for Atg11–Atg32 interaction and mitophagy. These findings suggest that mitophagy induction is strictly regulated by controlling the phosphorylation level of Ser-114 on Atg32.

RESULTS

The C-terminus region of Atg11 interacts with the N-terminus region (51–150) of Atg32

When autophagy selects mitochondria as a cargo, Atg11 interacts with a mitochondrial outer membrane localizing receptor Atg32 and recruits mitochondria to the PAS (Kanki *et al.*, 2009c; Okamoto *et al.*, 2009b). Because it has been reported that the C-terminus region of Atg11, including the fourth coiled-coil domain (CC4), interacts with the Cvt pathway receptor Atg19 (Yorimitsu and Klionsky, 2005), we speculated that the same region of Atg11 interacts with Atg32. To examine this possibility, we prepared a yeast two-hybrid construct to express Atg11 mutants fused with the Gal4 DNA-binding domain (BD-Atg11), activation domain–fused Atg32 (AD-Atg32), and activation domain–fused Atg19 (AD-Atg19). As previously reported, the cells expressing AD-Atg19 and BD-Atg11_CC4 (C-terminus region of Atg11 including CC4) grew on the selective plates, while the cells expressing AD-Atg19 and BD-Atg11_ΔCC4 (N-terminus region of Atg11 lacking CC4) did not grow on selective plates (Figure 1A; Yorimitsu and Klionsky, 2005). Similarly, the cells expressing AD-Atg32 and BD-Atg11_CC4, but not BD-Atg11_ΔCC4, grew on selective plates, suggesting that only the C-terminus region of Atg11 interacts with Atg32 (Figure 1A). To further examine the interaction between truncated Atg11 and Atg32, we expressed the constructs with hemagglutinin (HA)-tagged Atg11_CC4 or HA-tagged Atg11_ΔCC4 with protein A (PA)-tagged Atg32 and performed a protein A affinity pull-down assay with immunoglobulin G (IgG)–Sepharose. As we previously reported, PA-Atg32 coprecipitated a substantial amount of HA-Atg11_wild type (WT; Kanki *et al.*, 2009c; Figure 1B). PA-Atg32 also coprecipitated HA-Atg11_CC4 but not HA-Atg11_ΔCC4 (Figure 1B), suggesting that only the C-terminus region of Atg11 interacts with Atg32.

To identify the residues of Atg32 that interact with Atg11, we prepared yeast two-hybrid constructs to express the N-terminus– and/or C-terminus–truncated form of Atg32. As shown in Figure 1C, the cells expressing BD-Atg11 and AD-Atg32 mutants including amino acid residues 51–150 (Atg32_WT, 1-200, 1-150, 51-200, 51-150, and 51-529) grew on the selective plates. On the other hand, the cells expressing BD-Atg11 and the AD-Atg32 mutant lacking amino acid residues 51–150 (Atg32_151-529) or the AD-Atg32 mutant lacking 75 amino acids in the N-terminus (Atg32_76-529) did not grow on the selective plates (Figure 1C). These findings suggest that the N-terminus region of Atg32, especially amino acid residues 51–150, is important for the interaction with Atg11 (Figure 1D).

Atg32 is phosphorylated when mitophagy is induced

Mitophagy is induced when cells are cultured in lactate medium (YPL) and then shifted to nitrogen starvation medium supplemented with glucose (SD-N), or when cells are cultured in YPL for more than 2 d (allowing growth to the postlogarithmic phase; Kanki and Klionsky, 2008). We found that the molecular mass of Atg32 was changed when mitophagy was induced by nitrogen starvation (Figure 2A) or by allowing cellular growth to the postlogarithmic phase (unpublished data). In WT cells, the molecular mass of Atg32 was decreased by 2 h of nitrogen starvation; Atg32 was degraded following nitrogen starvation (Figure 2A, WT). In *atg11*Δ or *atg1*Δ cells, Atg32 was not degraded by nitrogen starvation (Figure 2A, *atg11*Δ; Supplemental Figure S1A), suggesting that Atg32 is degraded by mitophagy during nitrogen starvation. In *atg11*Δ cells, the molecular mass of Atg32 was decreased once (at 2 h) and then increased (at 4 and 6 h) during nitrogen starvation (Figure 2A, *atg11*Δ). To determine whether these molecular mass shifts were due to Atg32

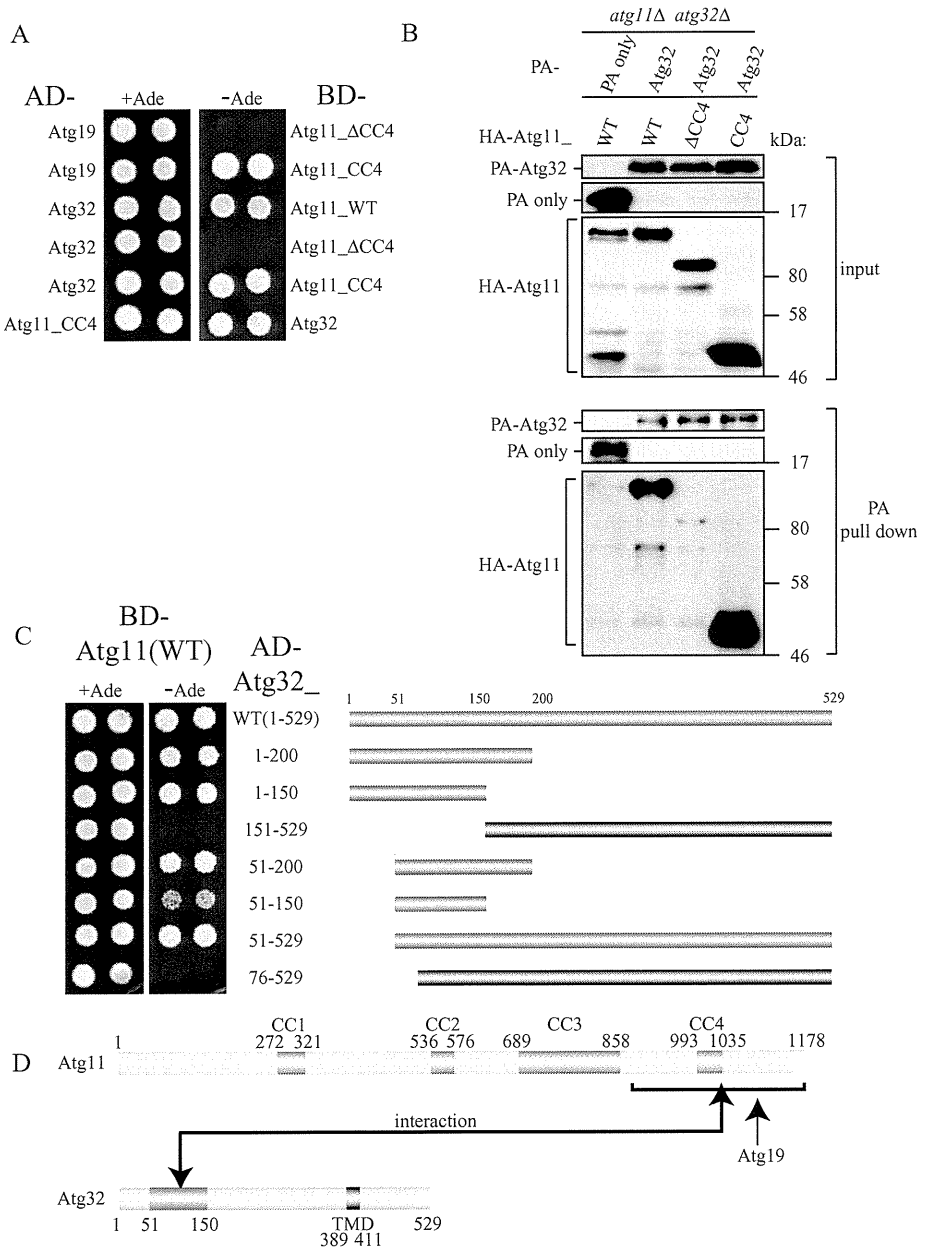

FIGURE 1: The N-terminus region (51–150) of Atg32 interacts with the C-terminus region of Atg11. (A) Yeast two-hybrid analysis between Atg19 and Atg11 mutants, and between Atg32 and Atg11 mutants. The PJ69-4A strain was transformed with pGAD and pGBD plasmid, which can express the indicated proteins. Cells were grown on +Ade or –Ade plates at 30°C for 4 d. (B) The C-terminus region of Atg11 associated with Atg32 during nitrogen starvation. The *atg11Δ atg32Δ* strains expressing PA-tagged Atg32 or PA only and the indicated HA-tagged Atg11 mutants under the control of the *CUP1* promoter were grown in SMD medium until the mid–log phase and then starved in SD-N for 1 h. PA-Atg32 was precipitated using IgG–Sepharose from cell lysates. Top two, an immunoblot of total-cell lysates. Bottom two, the IgG precipitates, which were probed with anti-HA and anti-PA antibodies. (C) Yeast two-hybrid analysis between Atg11 and the indicated Atg32 mutants (left). Each bar indicates expressed Atg32 mutants (right). Red bars indicate yeast two-hybrid positive and the gray bars indicate yeast two-hybrid negative. (D) Schematic drawing of Atg11 and Atg32. Atg11 is predicted to have a fourth coiled-coil domain (CC1–CC4). Atg32 has a TMD. The domain of Atg32 required for Atg11 interaction as determined by yeast two-hybrid study is highlighted in red.

phosphorylation, cellular protein extracts were treated with λ protein phosphatase (λ PPase) and the Atg32 molecular mass was observed. The molecular mass of Atg32 was decreased by λ PPase treatment before and after 6 h of nitrogen starvation (Figure 2B). Therefore we concluded that Atg32 is phosphorylated even in growing conditions in YPL medium, and after nitrogen starvation, Atg32 is dephosphorylated once and then is phosphorylated on two or three residues, depending on the nitrogen starvation period (Figure 2A, schematic model).

Phosphorylation of Ser-114 and Ser-119 on Atg32

To determine the phosphorylated residues in Atg32, we created Atg32 single–amino acid mutant expression vectors in which a Ser or Thr residue was altered to Ala (all created mutants are summarized in Supplemental Figure S1B), and those mutants were expressed in *ATG32* and *ATG11* double-deletion cells (*atg32Δ atg11Δ* cells), and Atg32 phosphorylation was observed during nitrogen starvation. We found that Atg32 with a mutation of Ser-114 to Ala or Ser-119 to Ala ($Atg32^{S114A}$ and $Atg32^{S119A}$, respectively) was not efficiently phosphorylated during nitrogen starvation (Figure 2C). Almost complete phosphorylation of $Atg32^{S119A}$ and partial $Atg32^{S114A}$ phosphorylation were inhibited at 1 h of nitrogen starvation compared with WT Atg32 ($Atg32^{WT}$; Figure 2C, SD-N, 1 h). At 6 h of nitrogen starvation, $Atg32^{S119A}$ phosphorylation was dramatically decreased compared with that of WT, although some phosphorylation remained (Figure 2C and Supplemental Figure S1C). $Atg32^{S114A}$ was phosphorylated to nearly identical levels as those of $Atg32^{WT}$ (Figure 2C and Supplemental Figure S1C). If both Ser-114 and Ser-119 were altered to Ala ($Atg32^{S114A/S119A}$), phosphorylation was almost completely inhibited, suggesting that phosphorylation observed in $Atg32^{S119A}$ at 6 h of nitrogen starvation is due to the phosphorylation of Ser-114 (Figure 2C and Supplemental Figure S1C). From these findings, we concluded that both Ser-114 and Ser-119 are phosphorylated by induction of mitophagy, although Ser-119 is more efficiently phosphorylated than Ser-114.

Phosphorylation of Atg32, especially phosphorylation of Ser-114 on Atg32, is critically important for mitophagy and for the Atg11–Atg32 interaction

If phosphorylation of Atg32 is necessary for mitophagy, we hypothesized that phosphorylation-deficient Atg32 mutants ($Atg32^{S114A}$, $Atg32^{S119A}$, and $Atg32^{S114A/S119A}$) are not functional for mitophagy. To observe mitophagy, we relied on the Om45–green fluorescent protein (GFP) processing assay, which can monitor mitophagy levels semiquantitatively (Kanki *et al.*, 2009a). Om45 is a mitochondrial outer membrane protein. We found that Om45 tagged with GFP (Om45-GFP)

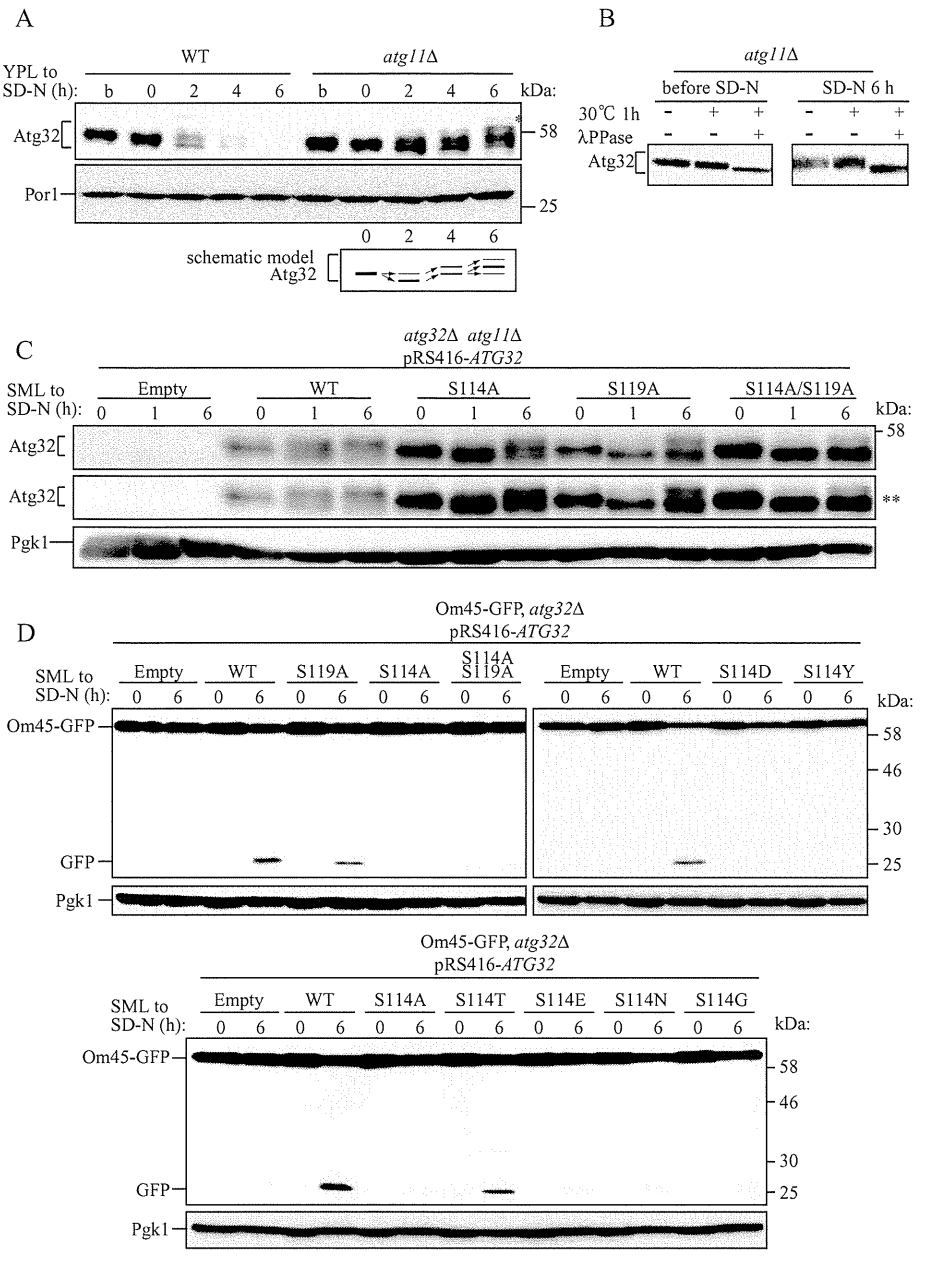

FIGURE 2: Phosphorylation of Atg32, especially phosphorylation of Ser-114 on Atg32, is essential for mitophagy. (A) WT or *atg11*Δ strains were cultured in YPL medium until the mid–log growth phase (indicated as b) and then shifted to SD-N medium for 0, 2, and 6 h. The amount and the modification of endogenous Atg32 were observed by immunoblotting with anti-Atg32 and anti-Por1 (loading control) antibodies. The variation in molecular weight of Atg32 in the *atg11*Δ strain is shown as a schematic model. The asterisk indicates a nonspecific band. (B) The *atg11*Δ strain was cultured in YPL medium until the mid–log growth phase (before SD-N) and then shifted to SD-N for 6 h. Cell lysates were treated with or without λ PPase at 30°C for 1 h. The molecular weight change was observed by immunoblotting with anti-Atg32 antibody. (C) The *atg32*Δ *atg11*Δ double-knockout strain transformed with vectors expressing the indicated *ATG32* mutants were cultured in YPL medium until the mid–log growth phase and then shifted to SD-N medium for 0, 1, and 6 h. The modification of Atg32 mutants was monitored by immunoblotting with anti-Atg32 and anti-Pgk1 (loading control) antibodies. The asterisks indicate a long exposure. (D) Strains of *atg32*Δ expressing Om45-GFP were transformed with the indicated Atg32 mutant-expressing vectors. Cells were cultured in SML medium until the mid–log growth phase and then shifted to SD-N for 6 h. GFP processing was monitored by immunoblotting with anti-GFP and anti-Pgk1 (loading control) antibodies.

was localized on the mitochondrial outer membrane and accumulated in vacuoles when mitophagy was induced. Om45-GFP that was accumulated in the vacuoles was degraded; however, the GFP was relatively stable within vacuoles and was often released as an intact protein. The level of mitophagy can be semiquantitatively monitored by measuring the amount of GFP processed from Om45-GFP using immunoblotting (Kanki and Klionsky, 2008; Kanki *et al.*, 2009a). We expressed $Atg32^{WT}$, $Atg32^{S114A}$, $Atg32^{S119A}$, and $Atg32^{S114A/S119A}$ in *atg32*Δ cells expressing Om45-GFP and induced mitophagy by nitrogen starvation or by allowing cellular growth to the postlogarithmic phase. Then we observed mitophagy using the Om45-GFP processing assay. When mitophagy was induced by nitrogen starvation, cells expressing $Atg32^{WT}$ showed substantial levels of GFP processing, whereas cells expressing $Atg32^{S119A}$ showed ~60% of GFP processing compared with WT. Cells expressing $Atg32^{S114A}$ or $Atg32^{S114A/S119A}$ did not show GFP processing (Figure 2D), suggesting that the S119A mutation partially affects the function of Atg32 for mitophagy and that the S114A mutation completely abolishes the function of Atg32. A similar result was observed if mitophagy was induced by allowing cellular growth up to the postlogarithmic phase (Supplemental Figure S2A). To exclude the possibility that the dysfunction of $Atg32^{S114A}$ is due to mislocalization of this protein, we expressed GFP-$Atg32^{WT}$ and GFP-$Atg32^{S114A}$ in the *atg32*Δ cells and observed Atg32 localization. As shown in Supplemental Figure S3, both GFP-$Atg32^{WT}$ and GFP-$Atg32^{S114A}$ were colocalized with MitoTracker Red, a probe for mitochondria, suggesting that S114A mutation does not affect Atg32 localization.

To distinguish whether dysfunction of $Atg32^{S114A}$ is due to the critical structural change of Atg32 or inability of Ser-114 phosphorylation, we constructed other Atg32 mutant expression vectors such as mutations of Ser-114 to Asn, Gly, Thr, Tyr, Asp, or Glu ($Atg32^{S114N}$, $Atg32^{S114G}$, $Atg32^{S114T}$, $Atg32^{S114Y}$, $Atg32^{S114D}$, or $Atg32^{S114E}$, respectively) and expressed these mutants in *atg32*Δ cells expressing Om45-GFP. Then we observed mitophagy. Because alternation of Ser to Asp or Glu can sometimes mimic the phosphorylated form of the protein, we expected that $Atg32^{S114D}$ or $Atg32^{S114E}$ might play a role in mitophagy, but both of these Atg32–mutant-expressing cells, as well as $Atg32^{S114N}$-, $Atg32^{S114G}$-, and $Atg32^{S114Y}$-expressing cells, did not show mitophagy (Figure 2D). Of interest, $Atg32^{S114T}$, which has the potential to be phosphorylated by Ser/Thr protein kinase, could induce mitophagy (Figure 2D), suggesting that phosphorylation of amino acid residue 114 of Atg32 is essential for mitophagy.

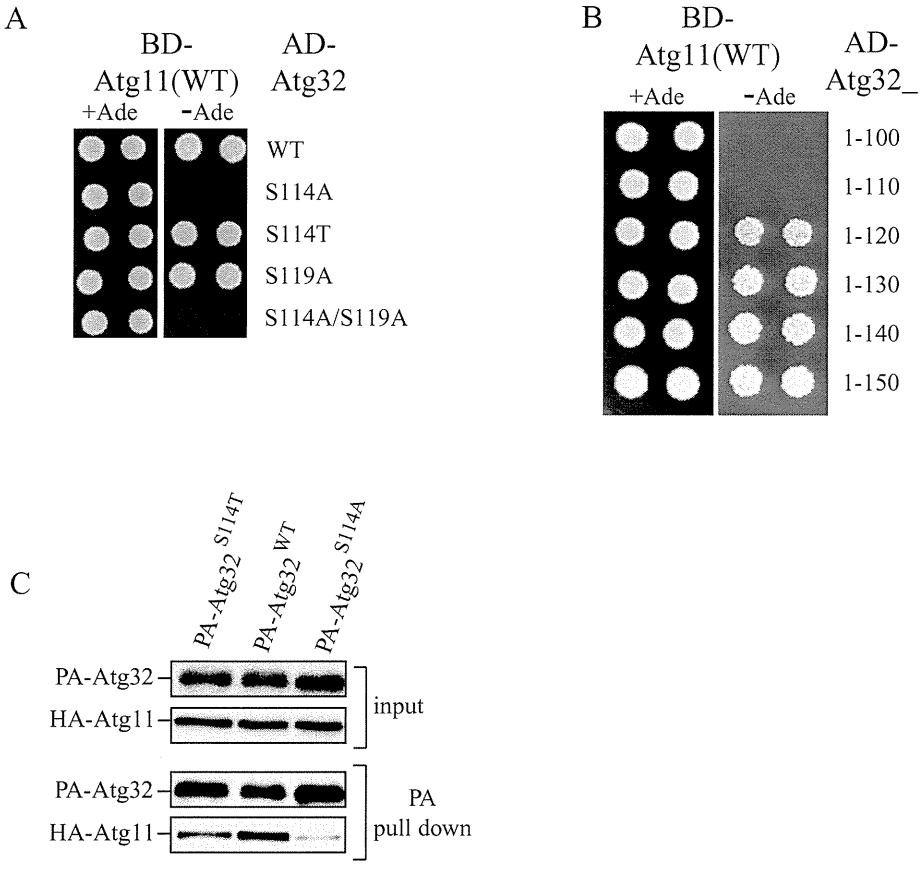

FIGURE 3: Phosphorylation of Ser-114 on Atg32 is critically important for the Atg11–Atg32 interaction. (A, B) Yeast two-hybrid analysis between Atg11 and the indicated Atg32 mutants. (C) The *atg11Δ atg32Δ* strains expressing PA-tagged Atg32^{WT}, PA-tagged Atg32^{S114A}, or PA-tagged Atg32^{S114T} and HA-tagged Atg11 under the control of the *CUP1* promoter were grown in SMD medium until the mid–log phase and then starved in SD-N for 1 h. PA-Atg32 was precipitated using IgG–Sepharose from cell lysates. Top two, an immunoblot of total-cell lysates. Bottom two, the IgG precipitates, which were probed with anti-HA and anti-PA antibodies.

Ser and Thr residues are clustered between Ser-114 and Ser-119 (Supplemental Figure S1B, green square). We further determined whether these Ser or Thr residues have an important role in mitophagy. We expressed Atg32^{S115A}, Atg32^{S116A}, Atg32^{D117A}, and Atg32^{T118A} in *atg32Δ* cells expressing Om45-GFP and observed mitophagy. All of those Atg32-mutant–expressing cells, however, showed a similar level of mitophagy with that of Atg32^{WT}-expressing cells (Supplemental Figure S2B).

Because phosphorylation of Ser-114 of Atg32 is necessary for mitophagy and because Ser-114 is within the Atg11 interaction region of Atg32 (Figure 1D, residues 51–150), we speculated that phosphorylation of Ser-114 might be necessary for the Atg11–Atg32 interaction. To examine this possibility, we prepared yeast two-hybrid constructs to express Atg32 phosphorylation-site mutants (AD-Atg32^{S114A}, AD-Atg32^{S119A}, AD-Atg32^{S114T}, and AD-Atg32$^{S114A/S119A}$). As expected, the cells expressing AD-Atg32^{S114A} or AD-Atg32$^{S114A/S119A}$ and BD-Atg11 did not grow, whereas AD-Atg32^{WT}, AD-Atg32^{S119A}, or AD-Atg32^{S114T} and BD-Atg11 did grow on selective plates (Figure 3A), suggesting that phosphorylation of Atg32-Ser-114 or Atg32-Thr114 is important for the Atg11–Atg32 interaction. We further studied the importance of the Ser-114 residue on the Atg11–Atg32 interaction. As shown in Figure 1C, the N-terminus 150 amino acids of Atg32 (Atg32_1-150) interacted with Atg11. We additionally prepared yeast two-hybrid Atg32 constructs to express N-terminus Atg32 including Ser-114 (Atg32_1-120, 1-130, 1-140, and 1-150) or N-terminus Atg32 excluding Ser-114 (Atg32_1-100 and 1-110). As expected, the cells expressing AD-Atg32 including Ser-114 (Atg32_1-120, 1-130, 1-140, and 1-150) and BD-Atg11 grew on the selective plates, whereas AD-Atg32 excluding Ser-114 (Atg32_1-100 and 1-110) and BD-Atg11 did not grow on the selective plates (Figure 3B). This finding further supports the idea that phosphorylation of Ser-114 on Atg32 is important for the Atg11–Atg32 interaction.

To confirm the importance of Atg32-Ser-114 phosphorylation on the Atg32–Atg11 interaction, we expressed HA-tagged Atg11 and PA-tagged Atg32^{S114A} or PA-tagged Atg32^{S114T} and performed a protein A affinity pull-down assay. PA-Atg32^{S114A} coprecipitated HA-Atg11 to a negligible extent compared with PA-Atg32^{WT} (Figure 3C). As expected, PA-Atg32^{S114T} could coprecipitate HA-Atg11, although the amount of HA-Atg11 coprecipitated with PA-Atg32^{S114T} was smaller than that with PA-Atg32^{WT} (Figure 3C). This finding further supports the idea that phosphorylation of Ser-114 (or Thr-114) in Atg32 is physiologically important for the Atg11–Atg32 interaction.

When mitophagy is induced, Atg11 interacts with Atg32 and recruits mitochondria to the PAS, which is formed on the vacuolar rim. We previously reported that GFP-Atg32^{WT} formed cytosolic GFP puncta at the PAS in an Atg11-dependent manner in the *atg1Δ* strain during nitrogen starvation (Kanki *et al.*, 2009c). Because phosphorylation of Ser-114 in Atg32 is important for the Atg11–Atg32 interaction, GFP-Atg32^{S114A} or GFP-Atg32$^{S114A/S119A}$ should not form GFP puncta at the PAS. To test this possibility, we expressed GFP-Atg32^{WT}, GFP-Atg32^{S114A}, and GFP-Atg32$^{S114A/S119A}$ in the *atg1Δ* and *atg32Δ* double-knockout strain and observed GFP puncta formation during nitrogen starvation. It was difficult to detect cytosolic GFP puncta in GFP-Atg32^{S114A}- or GFP-Atg32$^{S114A/S119A}$-expressing cells (only 4.5 and 2.0% of cells had puncta on the vacuolar rim during starvation, respectively), whereas cells expressing GFP-Atg32^{WT} showed cytosolic GFP puncta on the vascular rim (36.6% of the cells had puncta on the vacuolar rim; Supplemental Figure S4). This finding also supports the idea that Ser-114 in Atg32 is important for mitophagy.

Phosphorylation of Ser-114 or Ser-119 on Atg32 is not required for Atg32–Atg8 interaction

It was reported that Atg32 interacts with Atg8 through the WQAI motif on Atg32 and that the Atg32–Atg8 interaction also plays role in mitophagy (Okamoto *et al.*, 2009b). Because phosphorylation of Ser-114 on Atg32 is required for mitophagy, we speculated that this phosphorylation might affect Atg32–Atg8 interaction. We examined this possibility by yeast two-hybrid analysis. As shown in Supplemental Figure S5A, cells expressing BD-Atg8 and AD-Atg32 mutants (Atg32^{S114A}, Atg32^{S119A}, and Atg32$^{S114A/S119A}$), as well as AD-Atg32^{WT}, grew on the selective plates. This finding suggests that

phosphorylation of Ser-114 or Ser-119 on Atg32 is not required for Atg32–Atg8 interaction.

Phosphorylation of Atg32 is partially affected by the carbon source in the starvation medium

Mitophagy is induced by nitrogen starvation after preculturing yeast in nonfermentable medium. However, the level of mitophagy induction varies depending on the carbon source supplemented in starvation medium. Mitophagy is efficiently induced by nitrogen starvation in SD-N, whereas mitophagy occurs at a very low level in starvation medium with lactate (SL-N; Kanki and Klionsky, 2008). We speculated that the carbon source that supplements the starvation medium might affect the phosphorylation of Atg32, and as a result, the level of mitophagy induction might vary. To examine this possibility, we observed the phosphorylation of Atg32 in SD-N or SL-N medium after preculturing yeast in SML. As we previously reported, mitophagy occurred at a very low level when mitophagy was induced by SL-N compared with induction by SD-N (Supplemental Figure S5B; Kanki and Klionsky, 2008). Although the phosphorylation of Atg32 was similar after 6 h of nitrogen starvation in both SD-N and SL-N, phosphorylation after 1 h of starvation was very low in SL-N medium compared with that in SD-N (Supplemental Figure S5C). Therefore we concluded that the carbon source supplemented in the starvation medium affects the phosphorylation of Atg32 during starvation in the early period and that the difference in phosphorylation of Atg32, in part, affects the level of mitophagy induced by the starvation medium supplemented with a different carbon source.

Deletion of *HOG1* or *PBS2* affects both Atg32 phosphorylation and mitophagy

To identify kinases that phosphorylate Atg32 when mitophagy is induced, we investigated kinase or kinase cofactors encoding gene-deleted yeast strains and observed Atg32 phosphorylation when mitophagy was induced by nitrogen starvation. We found two kinases, Hog1 and Pbs2, related to Atg32 phosphorylation. Hog1 is a mitogen-activated protein kinase (MAPK), and Pbs2 is a mitogen-activated protein kinase kinase (MAPKK), and they are involved in the osmoregulatory signal transduction cascade (HOG signaling pathway), which affects gene expression by regulating osmoresponsive transcription factors (Westfall *et al.*, 2004). In both *HOG1*- and *PBS2*-deleted cells (*hog1*Δ and *pbs2*Δ cells, respectively), phosphorylation of Atg32 was severely but not completely inhibited when mitophagy was induced by nitrogen starvation (Figure 4A and Supplemental Figure S6A). Because phosphorylation of Atg32 is required for mitophagy, we speculated that mitophagy might be defective in *hog1*Δ and *pbs2*Δ cells. To test this possibility, we monitored mitophagy using the Om45-GFP processing assay and found that mitophagy was also severely defective in these cells (Figure 4B).

We further observed macroautophagy, the Cvt pathway, and pexophagy in *hog1*Δ and *pbs2*Δ cells. To observe macroautophagy, we used a Pho8Δ60 activity assay (Noda *et al.*, 1995). Pho8Δ60 is a truncated form of the vacuolar alkaline phosphatase. Deletion of the native signal sequence causes the precursor protein to remain in the cytosol, and it is only delivered to the vacuole by an autophagic mechanism. On delivery, the C-terminal propeptide is removed, resulting in activation of the zymogen, which can be measured enzymatically. We found that both *hog1*Δ and *pbs2*Δ cells, as well as WT cells, showed a similar increase in Pho8Δ60-dependent alkaline phosphatase activity following nitrogen starvation (Figure 4C). Consistent with previous reports that nitrogen starvation–induced macroautophagy is normal in the *HOG1* deleted strain under normoosmotic culture conditions (Prick *et al.*, 2006), our finding suggests that macroautophagy is not defective in the *hog1*Δ and *pbs2*Δ strains. This finding excludes the possibility that inhibition of mitophagy in *hog1*Δ and *pbs2*Δ cells is due to dysfunction of autophagic machinery. To observe the Cvt pathway, we investigated processing of the precursor from Ape1 (preApe1) under steady-state conditions. As shown in Figure 4D, preApe1 in *hog1*Δ and *pbs2*Δ cells was processed to comparable levels with those in WT cells, suggesting that the Cvt pathway is normal in *hog1*Δ and *pbs2*Δ cells. Finally, we used GFP processing from peroxisomal protein Pex14 tagged with GFP (Pex14-GFP) to observe pexophagy (Reggiori *et al.*, 2005). As shown in Figure 4E, pexophagy was severely defective in both *hog1*Δ and *pbs2*Δ cells. These findings suggest that the HOG signaling pathway is not related to the autophagic process but is related to regulation of organelle specific selective autophagy.

Because Hog1 is a kinase, we expected that Hog1 might directly phosphorylate Atg32. To observe this possibility, we challenged with an in vitro Hog1 kinase assay. Purified Hog1 was activated by a purified constitutive active Pbs2-EE mutant, and then purified Sko1 (N-terminus 214 amino acids; positive control) (Proft *et al.*, 2001) or purified Atg32 (N-terminus 250 amino acids) and [γ-^{32}P]ATP were mixed and incubated in vitro. As shown in Figure 4F, Sko1 was phosphorylated by Hog1, whereas Atg32 was not phosphorylated at all. This finding suggests that Atg32 is not directly phosphorylated by Hog1.

We then decided to determine whether components upstream of the HOG signaling pathway are required for mitophagy. Upstream of the HOG signaling pathway, there are two osmosensor complexes, Sho1–Msb2 and Sln1–Ypd1–Ssk1, and a layer of three MAPKKKs (Ssk2, Ssk22, and Ste11), which are responsible for activation of Pbs2 (Clotet and Posas, 2007). We expressed Om45-GFP in *sho1*Δ, *ste11*Δ, *ssk1*Δ, *msb2*Δ, *ssk2*Δ, and *ssk22*Δ cells and observed mitophagy. As shown in Supplemental Figure S6B, none of those mutants affected mitophagy, suggesting that, in the HOG signaling pathway, only Pbs2 and Hog1 are related to mitophagy. This result is consistent with the finding that hyperosmotic stress alone is not sufficient to induce mitophagy (Supplemental Figure S7A).

Finally, we observed whether Hog1 is activated under mitophagy-inducing conditions (Supplemental Figure S7B). As previously reported, Hog1 is phosphorylated (activated) by hyperosmotic stress (YPD + NaCl). Hog1 is also phosphorylated by nitrogen starvation (SD-N) but not by rapamycin (Rap) treatment (YPD + Rap). Of interest, Hog1 was strongly phosphorylated at the early log phase in YPL medium (preculture in YPL). During mitophagy, the phosphorylation of Hog1 was decreased but remained to some extent (SD-N). Surprisingly, when mitophagy was induced by rapamycin, the phosphorylation of Hog1 almost completely disappeared (YPL + Rap). These findings are consistent with the finding that Hog1 does not phosphorylate Atg32 directly and suggest that Hog1 is not the sole factor for Atg32 phosphorylation and mitophagy.

The N-terminus region of Atg32, especially the amino acids 51–100 of Atg32, contributes to stable expression of Atg32 but does not play a role in mitophagy

As shown in Figure 1C, when the first 50 amino acids in the N-terminus of Atg32 were deleted (51–529), this mutant could interact with Atg11 by yeast two-hybrid assay, whereas deletion of 75 amino acids in the N-terminus of Atg32 (76–529) could not. Therefore, we decided to address the function of the N-terminus region of Atg32. We first expressed N-terminus 50, 100, or 150 amino acid–deleted

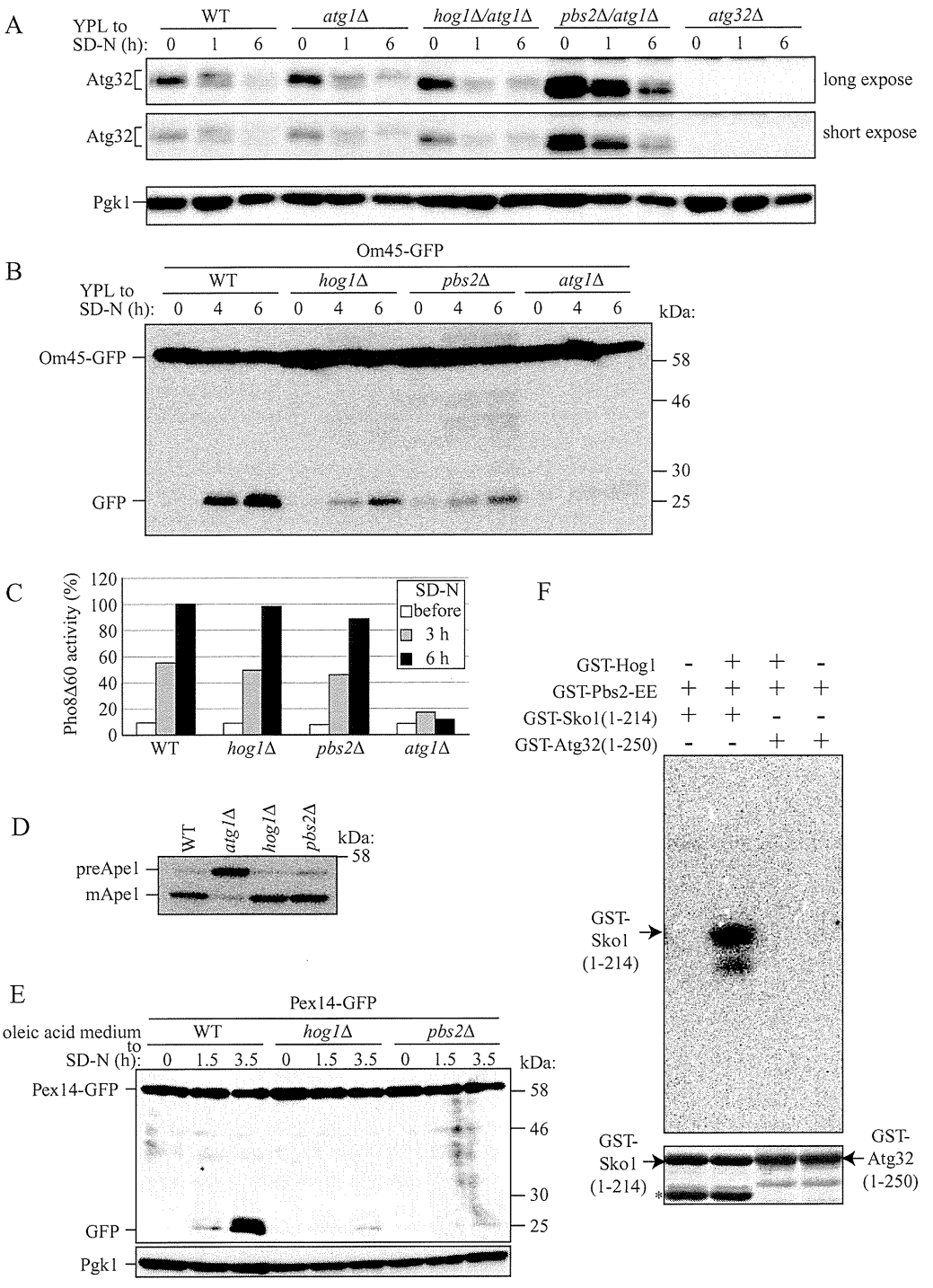

FIGURE 4: Deletion of *HOG1* or *PBS2* affects both Atg32 phosphorylation and mitophagy. (A) WT, *atg1*Δ, and *atg32*Δ strains and *hog1*Δ/ *atg1*Δ and *pbs2*Δ/*atg1*Δ double-knockout strains were cultured in YPL medium until the mid–log growth phase and then shifted to SD-N medium for 0, 1, and 6 h. Phosphorylation on endogenous Atg32 was monitored by immunoblotting with anti-Atg32 and anti-Pgk1 (loading control) antibodies. (B) Strains deleted for the indicated genes and expressing Om45-GFP were cultured in YPL medium until the mid–log growth phase and then shifted to SD-N for 4 and 6 h. GFP processing was monitored by immunoblotting with anti-GFP antibody. (C) The WT (TKMY236), *hog1*Δ (TKYM248), *pbs2*Δ (TKYM249), and *atg1*Δ (TKYM256) strains were grown in YPD medium and shifted to SD-N for 3 and 6 h. Samples were collected and protein extracts assayed for Pho8Δ60 activity. (D) WT, *atg1*Δ, *hog1*Δ, and *pbs2*Δ strains were cultured in YPD medium and analyzed for prApe1 maturation by immunoblotting with anti-Ape1 antiserum. (E) Strains deleted for the indicated genes and expressing Pex14-GFP were cultured with oleic acid–containing medium for 19 h and then shifted to SD-N for the indicated times and monitored for GFP processing by immunoblotting. (F) In vitro phosphorylation of Sko1(1-214) and Atg32(1-250) by Hog1. Recombinant GST-Sko1(1-214) or GST-Atg32(1-250) was phosphorylated by activated recombinant GST-Hog1 in the presence of [γ-^{32}P]ATP. The labeled proteins were resolved by SDS–PAGE, and an autoradiograph image (top) and Coomassie Brilliant Blue–stained image (bottom) of the gel were taken. The asterisks indicate GST-Sko1 degradation product or nonspecific bands.

Atg32 mutants (Atg32_51-529, 101-529, or 151-529) in *atg32Δ* cells expressing Om45-GFP and observed mitophagy during nitrogen starvation. Atg32_51-529–expressing cells showed comparable levels of GFP processing with those of Atg32_WT (Supplemental Figure S8A), suggesting that Atg32_51-529 is functional. Atg32_101-529–expressing cells showed a small amount of GFP processing, whereas Atg32_151-529–expressing cells completely lost GFP processing (Supplemental Figure S8A), suggesting that Atg32_101-529 can still slightly function. We also observed the expression levels of those Atg32 mutants and found that Atg32_101-529 was barely expressed compared with Atg32_WT or Atg32_51-529 (Supplemental Figure S8B). Therefore, we speculate that the N-terminus region of Atg32 might be required for stable expression of Atg32. To test this possibility, we additionally expressed N-terminus 69, 71, 73, or 75 amino acid–deleted Atg32 mutants (Atg32_70-529, 72-529, 74-529, or 76-529) in *atg32Δ* cells. Depending on the length deleted, the expression level of the Atg32 mutant was decreased, and when 75 amino acids were deleted in the N-terminus (Atg32_76-529), the expression level decreased to the same level of Atg32_101-529 (Supplemental Figure S8B). We then examined the function of these Atg32 mutants for mitophagy using the Om45-GFP processing assay. In response to the reduction of Atg32 mutant expression levels, GFP processing was decreased (compared with results shown in Supplemental Figures S8B and S8C), suggesting that the Atg32 mutant expression level, but not the length of N-terminus residues deleted, affects the level of mitophagy. To determine whether Atg32_76-529 or Atg32_101-529 is functional if the expression level is maintained, we expressed these mutants under the *CUP1* promoter, which can express genes more strongly than the Atg32 endogenous promoter. Under the *CUP1* promoter, Atg32_76-529 and Atg32_101-529 expressed comparable levels with those of full-length Atg32 expressed under the endogenous promoter (Supplemental Figure S9A). Cells expressing a substantial amount of Atg32_76-529 or Atg32_101-529 showed a similar level of mitophagy to that of full-length-Atg32–expressing cells (Supplemental Figure S9B). In addition, we constructed Atg32 lacking the amino acids 51–75 (Atg32_Δ51-75). Atg32_Δ51-75 was expressed at similar levels to those of full-length Atg32 (Supplemental Figure S9C), and cells expressing Atg32_Δ51-75 showed similar levels of mitophagy to those of full-length-Atg32–expressing cells (Supplemental Figure S9D). From these findings, we concluded that the N-terminus region of Atg32, especially the amino acids 51–100 of Atg32, contributes to stable expression of Atg32 but does not play a role in mitophagy.

The C-terminus region of Atg32, which is located in the inter membrane space, does not play a significant role in mitophagy

Atg32 is a single-span mitochondrial outer membrane protein with its N- and C-terminal domains oriented toward the cytoplasm and the intermembrane space, respectively. The transmembrane domain (TMD) is predicted to be from Ser-389 to Val-411 (Figure 1D). As shown in the preceding section, the N-terminus part of Atg32 interacts with Atg11, and this is essential for mitophagy. We next decided to address the role of the C-terminus region of Atg32 in mitophagy. We created a 100–amino acid deletion of the C-terminus of Atg32 that maintained the whole TMD (Atg32_ΔC100), a 120–amino acid deletion of the C-terminus of Atg32 that lacked part of the TMD (Atg32_ΔC120), and a 141–amino acid deletion of the C-terminus of Atg32 that completely lacked the TMD (Atg32_ΔC141). To observe mitophagy, we expressed those mutants in *atg32Δ* cells expressing Om45-GFP and induced mitophagy

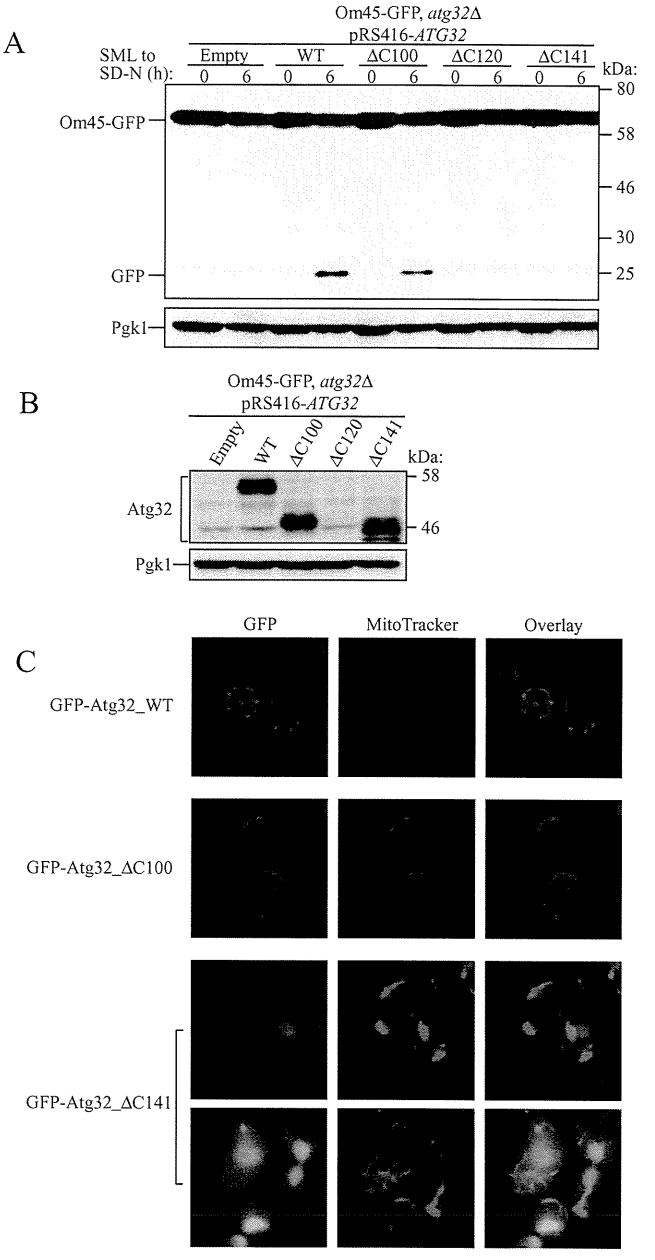

FIGURE 5: Characterization of the C-terminus region of Atg32. (A) Strains of *atg32Δ* expressing Om45-GFP were transformed with the indicated Atg32 mutant–expressing vectors. Cells were cultured in SML medium until the mid–log growth phase and then shifted to SD-N for 6 h. GFP processing was monitored by immunoblotting with anti-GFP and anti-Pgk1 (loading control) antibodies. (B) The same cells shown in A were cultured in SML medium until the mid–log growth phase. The expression level of Atg32 was observed by immunoblotting with anti-Atg32 and anti-Pgk1 (loading control) antibodies. (C) The wild-type strain transformed with a plasmid expressing the indicated GFP-tagged Atg32 mutants under the control of the *CUP1* promoter was cultured in SMD medium until the mid–log growth phase. Cells were labeled with the mitochondrial marker MitoTracker Red and analyzed by fluorescence microscopy.

by nitrogen starvation. Surprisingly, cells expressing Atg32_ΔC100 showed comparable levels of mitophagy to those of full-length Atg32, whereas cells expressing Atg32_ΔC120 or Atg32_ΔC141 showed a complete inhibition of mitophagy (Figure 5A). We then examined the expression level of Atg32 mutants. Both Atg32_ΔC100

and Atg32_ΔC141 were expressed to the same levels as those with full-length Atg32, but Atg32_ΔC120 was barely expressed (Figure 5B). We further observed mitochondrial localization of those Atg32 mutants by tagging GFP on its N-terminus. Similar to full-length Atg32, Atg32_ΔC100 was localized in the mitochondria, but, as expected, Atg32_ΔC141, which completely lacked TMD, was not localized in mitochondria (Figure 5C). From these findings, we concluded that the C-terminus region of Atg32 does not play a significant role in mitophagy, whereas the TMD is essential for Atg32 localization in mitochondria.

DISCUSSION

Mitochondria are organelles that supply energy to the cell. However, these organelles are also the major source of cellular ROS. Therefore quality control of mitochondria is important to maintain cellular homeostasis. Selective elimination of mitochondria via autophagy is believed to be a primary mechanism for mitochondrial quality control. Accordingly, it is important to understand the molecular mechanism of mitophagy and its regulation. Recent studies in yeast identified several mitophagy-related genes and showed that when autophagy selects mitochondria as a cargo, mitochondrial receptor protein Atg32 is recognized and bound by adaptor protein Atg11. Atg11 then recruits mitochondria to the PAS, where there is autophagosome uptake in the mitochondria (Kanki and Klionsky, 2009, 2010; Kanki *et al.*, 2009b, 2009c, 2010, 2011; Okamoto *et al.*, 2009a, 2009b). The Atg11–Atg32 interaction is believed to be the initial molecular process of mitophagy. It is unknown how the Atg11–Atg32 interaction is mediated or what signaling regulates it. In this study, we found that the C-terminus region of Atg11 (Atg11_CC4) interacts with the N-terminus region of Atg32 when mitophagy is induced. We also found that Atg32 is phosphorylated mainly on Ser-114 and Ser-119 following mitophagy induction and that the phosphorylation, especially phosphorylation of Ser-114, is necessary for the Atg11–Atg32 interaction and for mitophagy. We attempted to identify the factors that regulate Atg32 phosphorylation, and we found that Hog1 and Pbs2 were related to Atg32 phosphorylation. Hog1 is a MAPK and Pbs2 is a MAPKK, and both are involved in the HOG signaling pathway. Based on the findings that Hog1 does not phosphorylate Atg32 directly (Figure 4F), is not always activated under mitophagy-inducing conditions (Supplemental Figure S7B), and regulates the expression of ~600 genes (O'Rourke and Herskowitz, 2004), we speculate that Hog1 is one of the factors that affects an unidentified primary mitophagy signaling pathway or affects unidentified kinase(s) that directly phosphorylate Atg32.

This study found that Atg32 was phosphorylated even when cells were cultured in the growing phase (Figure 2, A and B). This unidentified phosphorylation site was dephosphorylated within 30 min by nitrogen starvation (unpublished data). This site phosphorylated in the growing phase is different from Ser-114 and Ser-119 because even $Atg32^{S114A/S119A}$ showed phosphorylation in the growing phase (Figure 2C). Until the current study, the physiological significance of this Atg32 phosphorylation and dephosphorylation on mitophagy was not well understood.

After nitrogen starvation, Atg32 was transiently dephosphorylated as discussed earlier and then phosphorylated on the residues of Ser-114 and Ser-119 (Figure 2, A and C). Although Ser-119 was more efficiently phosphorylated than Ser-114, phosphorylation of Ser-114 was strongly related to mitophagy (Figure 2D). Even if Ser-114 was altered to Thr, the Atg32 mutant ($Atg32^{S114T}$) was still functional for mitophagy, whereas the change of Ser-114 to Tyr completely disabled Atg32 function (Figure 2D). These findings strongly support our conclusion that a Ser/Thr–specific protein kinase phosphorylates Atg32 and that phosphorylation of the amino acid residue 114 of Atg32 is required for mitophagy.

Contrary to our expectation, neither $Atg32^{S114D}$ nor $Atg32^{S114E}$ was functional for mitophagy (Figure 2D). The substitution Ser to Asp or Glu is commonly used to mimic the phosphorylation status of protein. However, there is no guarantee that an acidic amino acid substitution will replicate the effect of phosphorylation since a phosphate group is considerably larger and carries twice the negative charge of a carboxylate (Cribbs and Strack, 2009). This might be the reason why neither $Atg32^{S114D}$ nor $Atg32^{S114E}$ was functional.

Mitophagy is inhibited even under strong macroautophagy-inducing nitrogen starvation conditions if the nitrogen starvation medium contains nonfermentable carbon as the sole carbon source in which mitochondria are essential for energy production (Kanki and Klionsky, 2008). We in addition found that the phosphorylation of Atg32 was affected by the carbon source supplemented in the starvation medium. These findings suggest that mitophagy is strictly regulated under an unidentified mitophagy-related signaling pathway. Phosphorylation of Ser-114 in Atg32 is likely to be the terminal reaction of this signaling pathway because phosphorylation of Atg32 directly mediates the Atg11–Atg32 interaction, which is the initial physical molecular step delivering mitochondria to vacuoles. The phosphorylation level of Ser-114 in Atg32 may be a rate-limiting factor of mitophagy.

Because Atg32 is evenly spread in the mitochondria (Kanki *et al.*, 2009c; Okamoto *et al.*, 2009b) and because mitochondria carrying phosphorylated Ser-114 in Atg32 are destined to be degraded, it is reasonable that the phosphorylation level of Ser-114 can be restricted to maintain a proper mitochondrial volume. In fact, we found that when mitophagy was induced by nitrogen starvation for 6 h, both degraded mitochondria and Ser-114 phosphorylation were consistently low (Figure 2D, SD-N 0 h compared with the 6 h Om45-GFP signal).

The current model for mitophagy is summarized in Figure 6. When mitophagy is induced, Ser-114 and Ser-119 on Atg32 are phosphorylated. The phosphorylation of Atg32, especially the phosphorylation of Ser-114, mediates the Atg11–Atg32 interaction. Atg11 recruits mitochondria to the PAS, where the autophagosome is generated to enclose the mitochondria. The kinase that directly phosphorylates Atg32 has not been identified yet (Figure 6, kinase X). The mitophagy signaling pathway that connects mitophagy-inducing stimuli derived from mitochondria and/or the cellular environment to kinase X is still unclear. It is possible that several factors related to the mitophagy signaling pathway, such as Hog1 and Pbs2, are involved.

The requirement of Atg32 phosphorylation for mitophagy is similar to pexophagy in *Pichia pastoris* because phosphorylation of PpAtg30, a receptor protein for pexophagy, is required for PpAtg30–PpAtg11 interaction and pexophagy (Farre *et al.*, 2008). Recently, it was reported that the MAPK Slt2 and upstream MAPK cascade are necessary for pexophagy in *Saccharomyces cerevisiae* (Manjithaya *et al.*, 2010). In the present study, we found that another MAPK, Hog1, and the upstream Pbs2 were required for mitophagy. Our study also showed that Hog1 was required for pexophagy (Figure 4F), whereas another study reported that it was not required for pexophagy (Manjithaya *et al.*, 2010). Although further studies are required to determine this issue, these findings suggest that there is an interaction between the MAPK cascade and selective autophagy in yeast.

We also studied the role of the first 100 amino acids of the N-terminus and C-terminus of Atg32 on mitophagy. Deletion of 100 amino acids in the C-terminus of Atg32, in which almost all of

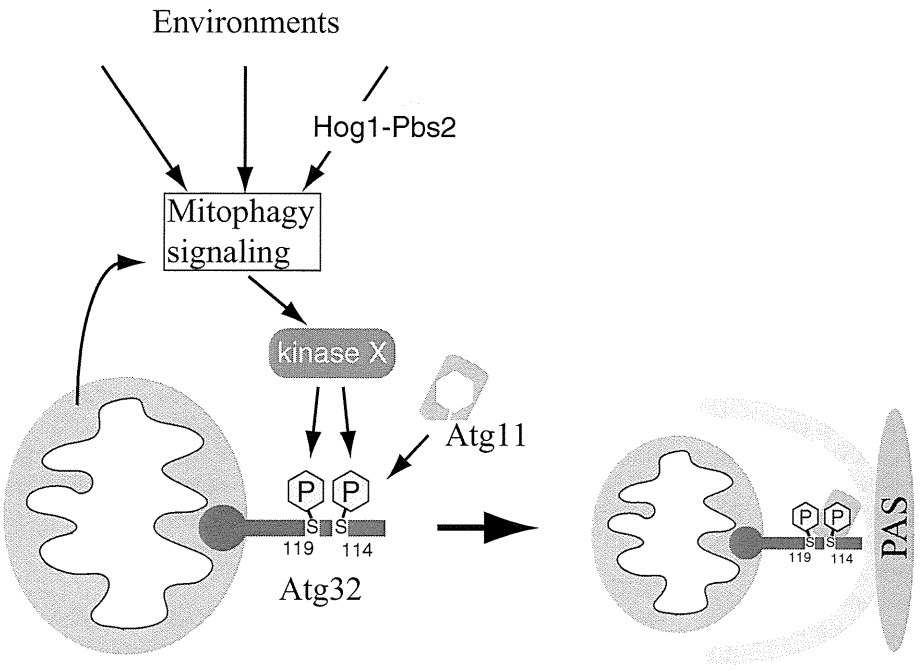

FIGURE 6: Model of mitophagy in yeast. The initial trigger-inducing mitophagy comes from mitochondria (such as mitochondrial damage) and/or the cellular environment (such as dramatic nutrient change and oxidative stresses). The initial trigger is through an unidentified mitophagy signaling pathway and it reaches kinase X, which is believed to be a Ser/Thr–specific protein kinase. This kinase phosphorylates Ser-114 and Ser-119 on Atg32. Phosphorylation of Atg32, especially phosphorylation of Ser-114, mediates the Atg11–Atg32 interaction. Atg11 recruits mitochondria to the PAS, where the autophagosome is generated to enclose the mitochondria. Hog1 and Pbs2 affect the mitophagy signaling pathway or affect kinase X.

the intermembrane space domain of Atg32 was deleted, resulted in mitophagy still being functional, suggesting that the C-terminus region of Atg32 does not play a role in mitophagy (at least under our mitophagy-inducing condition). On the other hand, we found that the N-terminus region of Atg32 was required for stable expression of Atg32, but it was not required for mitophagy. When more than 50 amino acids in the N-terminus of Atg32 were deleted, the expression level of Atg32 was decreased, depending on the length of the deleted residues (Supplemental Figure S8B). In response to the reduction of Atg32 mutant expression, induction of mitophagy was also decreased in parallel. This finding is consistent with previous reports that *N*-acetylcysteine, a scavenger of free radicals, suppresses the expression level of Atg32 (Okamoto *et al.*, 2009b) and mitophagy (Deffieu *et al.*, 2009). Atg32 lacking 100 amino acids in the N-terminus could induce mitophagy comparable with that in WT Atg32 if this mutant was expressed to the same level as that of endogenous WT Atg32 (Supplemental Figure S9, A and B), suggesting that the first 100 amino acids in the N-terminus of Atg32 are not involved in the molecular process of mitophagy. Because the Atg11–Atg32 interaction is essential for mitophagy, these 100 amino acids in the N-terminus of Atg32 can be excluded as the Atg11-interacting domain. Together with the yeast two-hybrid result that 120 amino acids in the N-terminus of Atg32 are sufficient to bind Atg11 (Figure 3B), this suggests that the Atg11 interaction region of Atg32 can be narrowed down as being amino acid residues 100–120.

MATERIALS AND METHODS

Strains and media

The yeast strains used in this study are listed in Supplemental Table S1. Yeast cells were grown in rich medium (YPD: 1% yeast extract, 2% peptone, and 2% glucose), lactate medium (YPL: 1% yeast extract, 2% peptone, and 2% lactate), synthetic minimal medium with glucose (SMD: 0.67% yeast nitrogen base, 2% glucose, and amino acids), or synthetic minimal medium with lactate (SML: 0.67% yeast nitrogen base, 2% lactate, and amino acids). Nitrogen starvation experiments were performed in synthetic minimal medium lacking nitrogen (SD-N: 0.17% yeast nitrogen base without amino acids and ammonium sulfate and 2% glucose; or SL-N: 0.17% yeast nitrogen base without amino acids and ammonium sulfate and 2% lactate).

Plasmids

The plasmids for expression of PA-tagged Atg32 (WT), GFP-tagged Atg32 (WT), and HA-tagged Atg11 mutants under the control of the *CUP1* promoter, the plasmids for expression of Atg32 (WT) under the endogenous promoter (pRS416-Atg32^{WT}), and yeast two-hybrid plasmid pGBDU-Atg11 mutants, pGAD-Atg19 and pGAD-Atg32 (WT), were described previously (Yorimitsu and Klionsky, 2005; Kanki *et al.*, 2009c). The plasmids expressing Atg32 with Ser or Thr mutation were generated using the QuikChange Site-Directed Mutagenesis Kit (Agilent Technologies, Santa Clara, CA) based on WT Atg32 expression plasmids. For the yeast two-hybrid vector pGAD-Atg32 mutants, a DNA fragment encoding N-terminus– or C-terminus–deleted *ATG32* was PCR amplified with *Bgl*II and *Sal*I restriction sites from yeast genomic DNA and ligated into the *Bam*HI and *Sal*I sites of pGAD-C1 (James *et al.*, 1996). For the N-terminus–deleted Atg32 expression vectors under the control of the endogenous Atg32 promoter, a DNA fragment encoding N-terminus–deleted *ATG32* was PCR amplified with the Atg32 promoter sequence from yeast genomic DNA and cotransfected with pRS416-Atg32^{WT} plasmid digested by *Bam*HI and *Afl*II in yeast (SEY6210) to allow recombination between the PCR fragment and digested plasmid. The objective plasmids were purified from the colonies grown on Ura (–) plates. For the C-terminus–deleted Atg32 expression vectors under the endogenous Atg32 promoter, a DNA fragment encoding promoter- and C-terminus–deleted *ATG32* was PCR amplified with *Spe*I and *Sal*I restriction sites from yeast genomic DNA and ligated into the *Spe*I and *Sal*I sites of the pRS416-CYC1tm vector (pRS416 vector with *CYC1* terminator). For the GFP-tagged C-terminus–deleted Atg32 expression vectors under the control of the *CUP1* promoter, a DNA fragment encoding C-terminus–deleted *ATG32* was PCR amplified with *Eco*RI and *Sal*I restriction sites from yeast genomic DNA and ligated into the *Eco*RI and *Sal*I sites of pCuGFP(416) (Kim *et al.*, 2001).

Antibodies

Anti-Atg32 antibody was produced by immunizing rabbits with the recombinant GST-tagged N-terminus (the first 400 amino acids) of Atg32 and affinity purifying the serum with recombinant His-tagged N-terminus (the first 250 amino acids) of Atg32-conjugated Sepharose. The affinity-purified anti-Atg32 antibody does not react with

the His-tagged N-terminus (the first 150 amino acids) of Atg32, suggesting that this antibody reacts with residues 151–250. Anti-ApeI antiserum was a gift from Daniel J. Klionsky (University of Michigan, Ann Arbor, MI). Anti-HA antibody (Sigma-Aldrich, St. Louis, MO), anti-Por1 antibody (Invitrogen Molecular Probes, Eugene, OR), anti-Pgk1 antibody (Nordic Immunological Laboratories, Tilburg, Netherlands), anti–protein A antibody (GeneTex, Irvine, CA), anti-Hog1 antibody (Santa Cruz Biotechnology, Santa Cruz, CA), anti–phosphorylated Hog1 antibody (Cell Signaling Technology, Beverly, MA), and anti-GFP antibody (Takara Bio, Otsu, Japan) were used for immunoblotting.

Assays for mitophagy, macroautophagy, the Cvt pathway, and pexophagy

For monitoring mitophagy, the Om45-GFP processing assay was carried out as described previously (Kanki *et al.*, 2009a). For monitoring macroautophagy, the alkaline phosphatase activity of Pho8Δ60 was measured as described previously (Noda *et al.*, 1995). For monitoring the Cvt pathway, cells were cultured in YPD medium up to the mid–log growth phase. The maturation of preApeI was observed by immunoblotting with anti-ApeI antiserum. For monitoring pexophagy, the Pex14-GFP processing assay was carried out as described previously (Reggiori *et al.*, 2005).

Protein A affinity pull-down assay

Cells expressing HA-tagged Atg11 (WT or mutants) and PA-tagged Atg32 (WT or mutants) were cultured in SMD medium until the mid–log growth phase and then shifted to SD-N for 1 h. Cells were collected and lysed with glass beads in IP buffer (50 mM 4-(2-hydroxyethyl)-1-piperazineethanesulfonic acid [HEPES], pH 7.4, 150 mM KCl, 1 mM EDTA, 0.5% Triton X-100, 1 mM phenylmethylsulfonyl fluoride [PMSF], and proteinase inhibitors), and they were centrifuged at 10,000 × *g* for 10 min at 4°C. The supernatant was mixed with IgG–Sepharose at 4°C for 12 h. The Sepharose was washed by ice-cold wash buffer (50 mM HEPES, pH 7.4, 500 mM NaCl, 1 mM EDTA, 0.5% Triton X-100, and 0.1% SDS) five times, and the sample was eluted by SDS–PAGE loading buffer. The elution samples were observed by immunoblotting with anti-HA and anti–protein A antibodies.

λ Protein phosphatase treatment

The *atg11*Δ strain was cultured in YPL medium until the mid–log phase and then shifted to SD-N for 6 h. Cells were collected and lysed with glass beads in phosphatase buffer (supplied with λ protein phosphatase) with 1 mM PMSF and protease inhibitors. After centrifugation at 10,000 × *g* for 10 min, the supernatant was incubated with λ protein phosphatase (New England BioLabs, Ipswich, MA) for 1 h at 30°C.

Fluorescence microscopy

Cells expressing GFP-tagged Atg32 mutants were grown in SMD medium until the mid–log growth phase. To label mitochondria, cells were incubated with 1 μM of MitoTracker Red (Invitrogen) at 30°C for 30 min. After cells were washed with SMD medium, fluorescence signals were visualized on a BZ-9000 fluorescence microscope (Keyence, Osaka, Japan). To observe cytosolic GFP puncta formation, cells were incubated with 20 μg/ml *N*-(3-triethylammoniumpropyl)-4-(*p*-diethylaminophenylhexatrienyl) pyridinium dibromide (FM 4-64; Biotium, Hayward, CA) at 30°C for 30 min. After being washed with sterilized water, the cells were incubated in SD-N for 2 h. The fluorescence signals were visualized on the A1R confocal laser microscope system (Nikon, Tokyo, Japan).

In vitro kinase assay

For the in vitro kinase assay, we used a method described previously (Bilsland-Marchesan *et al.*, 2000; Proft *et al.*, 2001). N-terminus GST-tagged Hog1, Pbs2-EE (Ser-514 to Glu and Thr-518 to Glu mutant), Sko1 (N-terminus 214 amino acids), and Atg32 (N-terminus 250 amino acids) expression vectors were constructed using pGEX-4T-1 (GE Healthcare, Chalfont St. Giles, United Kingdom) and were expressed in *Escherichia coli* BL21(DE3). Expressed proteins were purified using Glutathione Sepharose 4B (GE Healthcare). One microgram of recombinant GST–Hog1 was activated by phosphorylation using 0.5 μg of GST–Pbs2-EE in the presence of kinase buffer (50 mM Tris-HCl, pH 7.5, 10 mM $MgCl_2$, and 2 mM dithiothreitol) and 20 μM ATP. After 20 min at 30°C, 2.5 μg of GST-Sko1 or GST-Atg32 was added to the previous mixture together with [γ-^{32}P]ATP (0.2 μCi/μl). The mixture was then incubated for 20 min at 30°C. The labeled proteins were resolved by SDS–PAGE. The gel was stained with Coomassie Brilliant Blue, and the gel images were visualized by BAS-2500 autoradiography (Fujifilm, Tokyo, Japan).

ACKNOWLEDGMENTS

We thank Daniel J. Klionsky (University of Michigan) for providing strains, plasmids, and antiserums and for helpful advice. This work was supported in part by a Grant-in-Aid for Young Scientists (A) (23689032) (T.K.), a Grant-in-Aid for Scientific Research on Priority Areas (22020028) (T.K.) and Scientific Research (A) (22249018) (D.K.) from the Ministry of Education, Culture, Sports, Science and Technology of Japan, as well as support from the Uehara Memorial Foundation (T.K.), the Takeda Science Foundation (T.K.), the Naito Foundation (T.K.), the Mochida Memorial Foundation for Medical and Pharmaceutical Research (T.K.), the Kowa Life Science Foundation (T.K.), and Kyushu University Interdisciplinary Programs in Education and Projects in Research Development (T.K.). We appreciate technical support from the Research Support Center, Graduate School of Medical Sciences, Kyushu University.

REFERENCES

Arai M, Imai H, Koumura T, Yoshida M, Emoto K, Umeda M, Chiba N, Nakagawa Y (1999). Mitochondrial phospholipid hydroperoxide glutathione peroxidase plays a major role in preventing oxidative injury to cells. J Biol Chem 274, 4924–4933.

Bilsland-Marchesan E, Arino J, Saito H, Sunnerhagen P, Posas F (2000). Rck2 kinase is a substrate for the osmotic stress-activated mitogen-activated protein kinase Hog1. Mol Cell Biol 20, 3887–3895.

Bogenhagen DF (1999). Repair of mtDNA in vertebrates. Am J Hum Genet 64, 1276–1281.

Clotet J, Posas F (2007). Control of cell cycle in response to osmostress: lessons from yeast. Methods Enzymol 428, 63–76.

Cribbs JT, Strack S (2009). Functional characterization of phosphorylation sites in dynamin-related protein 1. Methods Enzymol 457, 231–253.

Deffieu M, Bhatia-Kissova I, Salin B, Galinier A, Manon S, Camougrand N (2009). Glutathione participates in the regulation of mitophagy in yeast. J Biol Chem 284, 14828–14837.

Elmore SP, Qian T, Grissom SF, Lemasters JJ (2001). The mitochondrial permeability transition initiates autophagy in rat hepatocytes. FASEB J 15, 2286–2287.

Farre JC, Manjithaya R, Mathewson RD, Subramani S (2008). PpAtg30 tags peroxisomes for turnover by selective autophagy. Dev Cell 14, 365–376.

Friguet B, Bulteau AL, Petropoulos I (2008). Mitochondrial protein quality control: implications in ageing. Biotechnol J 3, 757–764.

Goldman SJ, Zhang Y, Jin S (2010). Autophagic degradation of mitochondria in white adipose tissue differentiation. Antioxid Redox Signal 14, 1971–1978.

James P, Halladay J, Craig EA (1996). Genomic libraries and a host strain designed for highly efficient two-hybrid selection in yeast. Genetics 144, 1425–1436.

Johansen T, Lamark T (2011). Selective autophagy mediated by autophagic adapter proteins. Autophagy 7, 279–296.

Kanki T, Kang D, Klionsky DJ (2009a). Monitoring mitophagy in yeast: the Om45-GFP processing assay. Autophagy 5, 1186–1189.
Kanki T, Klionsky D, Okamoto K (2011). Mitochondria autophagy in yeast. Antioxid Redox Signal 14, 1989–2001.
Kanki T, Klionsky DJ (2008). Mitophagy in yeast occurs through a selective mechanism. J Biol Chem 283, 32386–32393.
Kanki T, Klionsky DJ (2009). Atg32 is a tag for mitochondria degradation in yeast. Autophagy 5, 1201–1202.
Kanki T, Klionsky DJ (2010). The molecular mechanism of mitochondria autophagy in yeast. Mol Microbiol 75, 795–800.
Kanki T *et al.* (2009b). A genomic screen for yeast mutants defective in selective mitochondria autophagy. Mol Biol Cell 20, 4730–4738.
Kanki T, Wang K, Cao Y, Baba M, Klionsky DJ (2009c). Atg32 is a mitochondrial protein that confers selectivity during mitophagy. Dev Cell 17, 98–109.
Kanki T, Wang K, Klionsky DJ (2010). A genomic screen for yeast mutants defective in mitophagy. Autophagy 6, 278–280.
Kim J, Kamada Y, Stromhaug PE, Guan J, Hefner-Gravink A, Baba M, Scott SV, Ohsumi Y, Dunn WA Jr, Klionsky DJ (2001). Cvt9/Gsa9 functions in sequestering selective cytosolic cargo destined for the vacuole. J Cell Biol 153, 381–396.
Klionsky DJ, Emr SD (2000). Autophagy as a regulated pathway of cellular degradation. Science 290, 1717–1721.
Larsson NG, Clayton DA (1995). Molecular genetic aspects of human mitochondrial disorders. Annu Rev Genet 29, 151–178.
Lemasters JJ (2005). Selective mitochondrial autophagy, or mitophagy, as a targeted defense against oxidative stress, mitochondrial dysfunction, and aging. Rejuvenation Res 8, 3–5.
Manjithaya R, Jain S, Farre JC, Subramani S (2010). A yeast MAPK cascade regulates pexophagy but not other autophagy pathways. J Cell Biol 189, 303–310.
Nakatogawa H, Suzuki K, Kamada Y, Ohsumi Y (2009). Dynamics and diversity in autophagy mechanisms: lessons from yeast. Nat Rev Mol Cell Biol 10, 458–467.
Narendra D, Tanaka A, Suen DF, Youle RJ (2008). Parkin is recruited selectively to impaired mitochondria and promotes their autophagy. J Cell Biol 183, 795–803.
Narendra DP, Jin SM, Tanaka A, Suen DF, Gautier CA, Shen J, Cookson MR, Youle RJ (2010). PINK1 is selectively stabilized on impaired mitochondria to activate Parkin. PLoS Biol 8, e1000298.
Narendra DP, Youle RJ (2011). Targeting mitochondrial dysfunction: role for PINK1 and Parkin in mitochondrial quality control. Antioxid Redox Signal 14, 1929–1938.
Noda T, Matsuura A, Wada Y, Ohsumi Y (1995). Novel system for monitoring autophagy in the yeast *Saccharomyces cerevisiae*. Biochem Biophys Res Commun 210, 126–132.
Nowikovsky K, Reipert S, Devenish RJ, Schweyen RJ (2007). Mdm38 protein depletion causes loss of mitochondrial K^+/H^+ exchange activity, osmotic swelling and mitophagy. Cell Death Differ 14, 1647–1656.
O'Rourke SM, Herskowitz I (2004). Unique and redundant roles for HOG MAPK pathway components as revealed by whole-genome expression analysis. Mol Biol Cell 15, 532–542.
Okamoto K, Kondo-Okamoto N, Ohsumi Y (2009a). A landmark protein essential for mitophagy: Atg32 recruits the autophagic machinery to mitochondria. Autophagy 5, 1203–1205.
Okamoto K, Kondo-Okamoto N, Ohsumi Y (2009b). Mitochondria-anchored receptor Atg32 mediates degradation of mitochondria via selective autophagy. Dev Cell 17, 87–97.
Oku M, Sakai Y (2010). Peroxisomes as dynamic organelles: autophagic degradation. FEBS J 277, 3289–3294.
Priault M, Salin B, Schaeffer J, Vallette FM, di Rago JP, Martinou JC (2005). Impairing the bioenergetic status and the biogenesis of mitochondria triggers mitophagy in yeast. Cell Death Differ 12, 1613–1621.
Prick T, Thumm M, Kohrer K, Haussinger D, Vom Dahl S (2006). In yeast, loss of Hog1 leads to osmosensitivity of autophagy. Biochem J 394, 153–161.
Proft M, Pascual-Ahuir A, de Nadal E, Arino J, Serrano R, Posas F (2001). Regulation of the Sko1 transcriptional repressor by the Hog1 MAP kinase in response to osmotic stress. EMBO J 20, 1123–1133.
Reggiori F, Monastyrska I, Shintani T, Klionsky DJ (2005). The actin cytoskeleton is required for selective types of autophagy, but not nonspecific autophagy, in the yeast *Saccharomyces cerevisiae*. Mol Biol Cell 16, 5843–5856.
Rep M, Grivell LA (1996). The role of protein degradation in mitochondrial function and biogenesis. Curr Genet 30, 367–380.
Rodriguez-Enriquez S, He L, Lemasters JJ (2004). Role of mitochondrial permeability transition pores in mitochondrial autophagy. Int J Biochem Cell Biol 36, 2463–2472.
Sandoval H, Thiagarajan P, Dasgupta SK, Schumacher A, Prchal JT, Chen M, Wang J (2008). Essential role for Nix in autophagic maturation of erythroid cells. Nature 454, 232–235.
Schweers RL *et al.* (2007). NIX is required for programmed mitochondrial clearance during reticulocyte maturation. Proc Natl Acad Sci USA 104, 19500–19505.
Shintani T, Huang WP, Stromhaug PE, Klionsky DJ (2002). Mechanism of cargo selection in the cytoplasm to vacuole targeting pathway. Dev Cell 3, 825–837.
Twig G *et al.* (2008). Fission and selective fusion govern mitochondrial segregation and elimination by autophagy. EMBO J 27, 433–446.
Voos W (2009). Mitochondrial protein homeostasis: the cooperative roles of chaperones and proteases. Res Microbiol 160, 718–725.
Wallace DC (2005). A mitochondrial paradigm of metabolic and degenerative diseases, aging, and cancer: a dawn for evolutionary medicine. Annu Rev Genet 39, 359–407.
Westfall PJ, Ballon DR, Thorner J (2004). When the stress of your environment makes you go HOG wild. Science 306, 1511–1512.
Yang Z, Klionsky DJ (2010). Eaten alive: a history of macroautophagy. Nat Cell Biol 12, 814–822.
Yorimitsu T, Klionsky DJ (2005). Atg11 links cargo to the vesicle-forming machinery in the cytoplasm to vacuole targeting pathway. Mol Biol Cell 16, 1593–1605.
Yuga M, Gomi K, Klionsky DJ, Shintani T (2011). Aspartyl aminopeptidase is imported from the cytoplasm to the vacuole by selective autophagy in *Saccharomyces cerevisiae*. J Biol Chem 286, 13704–13713.

Cancer Science
The official journal of the Japanese Cancer Association JCA

Mitochondrial p32/C1QBP is highly expressed in prostate cancer and is associated with shorter prostate-specific antigen relapse time after radical prostatectomy

Rie Amamoto,[1,2] Mikako Yagi,[1] YooHyun Song,[3,4] Yoshinao Oda,[3] Masazumi Tsuneyoshi,[3] Seiji Naito,[4] Akira Yokomizo,[4] Kentaro Kuroiwa,[4] Shoji Tokunaga,[5] Seiji Kato,[6] Hisahide Hiura,[6] Tomohiro Samori,[6] Dongchon Kang[1,7] and Takeshi Uchiumi[1,7]

[1]Department of Clinical Chemistry and Laboratory Medicine, Graduate School of Medical Sciences, Kyushu University, Fukuoka; [2]Department of Nutritional Sciences, Faculty of Health and Welfare, Seinan Jo Gakuin University, Kitakyushu; Departments of [3]Anatomic Pathology, [4]Urology, Graduate School of Medical Sciences, Kyushu University, Fukuoka; [5]Department of Medical Informatics, Kyushu University Hospital, Fukuoka; [6]Research Division, Japan Clinical Laboratories, Inc., Kyoto, Japan

(Received August 9, 2010/Revised December 1, 2010/Accepted December 2, 2010/Accepted manuscript online December 9, 2010/Article first published online January 23, 2011)

Mitochondria are key organelles for ATP production and apoptosis. Therefore, impairment of mitochondria can modulate or accelerate cancer progression. p32, originally identified as a pre-mRNA splicing factor SF2/ASF-associated protein, is localized predominantly in the mitochondrial matrix and involved in mitochondria respiration. Recently, p32 was implicated in apoptosis and resultantly cancer progression. However, little is known about the expression and function of p32 in human tumors including prostate cancer. Here, we investigated the expression of p32 in 148 prostate carcinoma tissues by immunohistochemistry and found a positive correlation of p32 expression to clinicopathological parameters including follow-up data. p32 is highly expressed in prostate tumor samples and its expression is significantly associated with the Gleason score, pathological stage and relapse. For localized cancers, high p32 is a strong and independent predictor of clinical recurrence in multivariate analysis ($P = 0.01$). In addition, p32 is overexpressed in the prostate cancer cell lines examined. The selective knockdown of p32 by RNA interference inhibits the growth of prostate cancer cell lines but not of a non-cancerous cell line. The p32 RNA interference decreases cyclin D1, increases p21 expression and causes a G1/S cell cycle arrest in prostate cancer cells. These data suggest that p32 is critical for prostate cancer cell proliferation and may be a novel marker of clinical progression in prostate cancer. (*Cancer Sci* 2011; 102: 639–647)

p32 (C1QBP/gC1qR/HABP1) was first isolated from a membrane preparation of Raji cells historically and was originally copurified with the pre-mRNA splicing factor SF2/ASF in human HeLa cell.[1–3] p32 protein is a doughnut-shaped trimer[4] that is primarily localized in the mitochondria,[1,5–7] but has also been reported to be present at the cell surface[6,8] and in the nucleus[5,9,10] Human p32 has been reported to interact with a variety of molecules including human immunodeficiency virus Tat, complement 1q (C1q) and hyaluronic acids.[11] These results suggest that p32 may be a multifunctional chaperone protein.[12] Recently, it was reported that p32 was implicated in mediating the cellular apoptotic response.[13] ARF interacts with p32 and the interaction is critical in order for ARF to localize to the mitochondria and induce apoptosis.[14,15] It has also been proposed that p32 is a link to autophagy.[16,17] However, the role of p32 in mammalian cancer cells is unclear.

Previously, we identified a *Saccharomyces cerevisiae* homologue of the human p32 gene, referred to as mam33, which was localized in the mitochondrial matrix. Disruption of the mam33 gene caused growth retardation and impairment of mitochondrial ATP synthesis. The growth impairment was restored by the introduction of human p32 cDNA, indicating that mam33 is a functional yeast counterpart of human p32. Taken together, both human p32 and yeast mam33 reside in the mitochondrial matrix and play an important role in maintaining mitochondrial oxidative phosphorylation.[1]

Prostate cancer is the second commonest cause of male cancer death in the developed world and is the most frequent from of malignancy diagnosed.[18,19] Various lifestyles and nutritional factors, particularly high-energy consumption, were reported in relation to a risk of prostate cancer.[18,20] In patients with locally advanced disease or metastatic cancer, androgen ablation remains the mainstay of treatment. However, the effect of this treatment is only transient, with most patients developing hormone-refractory disease within 2–3 years. A better understanding of the mechanism involved in regulating tumor growth and the identification of novel growth factors implicated in disease progression would be useful to develop new therapeutic approaches. Currently, there are few markers clinically available for accurate prediction of the prognosis of prostate cancer patients besides prostate-specific antigen (PSA) and Gleason score.[21]

The metabolic phenotype is characterized by a shift from oxidative phosphorylation (OXPHOS) towards aerobic glycolysis as the main source of ATP production, a phenomenon first described by Warburg.[22] It is now recognized that the Warburg effect represents a prominent metabolic characteristic of malignant cells. Although Warburg has speculated that mitochondrial respiration is decreased in cancer cells, mitochondrial activity is essential for cancer cell survival. The mitochondria also participates in many essential and fundamental metabolic pathways including the synthesis of pyrimidine through dihydroorotate dehydrogenase (DHODH) in addition to respiration.[23]

The cell cycle phases are coordinated by the expression and/or activation of regulatory proteins, including cyclins (e.g. cyclins D, E and A), cyclin-dependent kinases (CDK) and cyclin-dependent kinase inhibitors (CDKIs).[24] CDK4 and CDK6 form complexes with one of several D-type cyclins and function early in the G1 phase. CDK2 complexed with cyclins A and E is essential for DNA replication and G1/S transition, respectively.[25] Five membrane-anchored protein complexes

[7]To whom correspondence should be addressed.
E-mail: uchiumi@cclm.med.kyushu-u.ac.jp; kang@cclm.med.kyushu-u.ac.jp

doi: 10.1111/j.1349-7006.2010.01828.x

(complex I–V) are the main machineries for mitochondrial oxidative phosphorylation, and defects in this process have been implicated in the progression of ageing and in diverse age-related disorders such as cancer and degenerative diseases. Thus, it has been broadly accepted that there is a close relationship between respiratory control and apoptosis/cell cycle progression.

Considering that p32 is a key molecule of oxidative phosphorylation and apoptosis in mitochondria, it might be involved in cancer progression. In fact, the expression levels of p32 were significantly increased in multiple human cancer tissues compared with normal tissues. In the current study, we investigated the expression of p32 in prostate carcinomas of patients by immunohistochemistry and found a strong correlation of the expression to clinicopathological parameters including follow-up data. We also investigated the expression of p32 in human cancer cell lines and examined the effects of its small interference RNA (siRNA)-mediated knockdown on cell proliferation and the cell cycle. Here we propose that mitochondrial matrix protein p32 may be a novel progressive marker in prostate cancer.

Materials and Methods

Patients, tissue and clinicopathological data. The subjects were 148 patients (age, 47–78 years; mean, 65.6 years), who received radical prostatectomy with no chemotherapy or hormonal therapy before surgery at the Kyushu University Hospital, Fukuoka, Japan, between 1997 and 2006 and had enough carcinoma area for evaluation of immunohistochemistry. All patients underwent surgery for clinically localized prostate cancer as determined by preoperative PSA concentration, digital rectal examination and prostate needle biopsy. Detailed clinicopathological findings of the patients are summarized in Supporting Information Table S1. All prostatectomy specimens were completely reviewed to establish stage and grade of the respective prostate cancers.[21] Four patients received adjuvant hormonal therapy after surgery. Sixteen patients had <2 years of follow up. Clinical follow-up data were available for 128 patients. Their serum PSA was monitored; a PSA level >4 ng/mL was defined as PSA recurrence. Prostate-specific antigen recurrence was found in 20% (26/128) of patients. The median follow-up time of patients still relapse-free at the end of analysis was 49.5 months.[19]

Antibody. Anti-TFAM were raised in our laboratory.[26] Anti-p32 mouse monoclonal antibody (clone1) was produced in the Japan Clinical Laboratories Incorporation (Kyoto, Japan). Anti-β-actin was purchased from Sigma–Aldrich (Steinheim, Germany). Anti-cyclinD1, p15INK4B, p21Waf1/cip1, p27kip1, CDK4 and CDK6 were purchased from Cell Signaling (Danvers, MA, USA) and anti-B23 was purchased from Invitrogen (San Diego, CA, USA).

Immunohistochemistry. Immunohistochemistry was performed using the streptavidin–biotin–peroxidase method with a Histofine streptavidin–biotin–peroxidase kit (Nichirei, Tokyo, Japan). The primary antibody used in the present study was anti-p32 antibody (mouse monoclonal IgG1, 13 μg/mL). The specificity of p32 antibodies was tested using pre-absorption with recombinant p32 antigens with optimally diluted antiserum overnight at 4°C (Supporting Information Fig. S1). Sections, 4-μm thick, from 10% formalin-fixed, paraffin-embedded material were deparaffinized in xylene and dehydrated through ethanol. Their endogenous peroxidase activity was then blocked by methanol containing 0.3% hydrogen peroxidase for 30 min. After the peroxidase activity blocking, the sections were immunized to 10% rabbit serum in phosphate-buffered saline for 10 min; the sections were incubated at room temperature for 2 h with anti-p32. Those sections were then incubated with the second antibody for 20 min at room temperature. The reaction products were visualized by 3,3′-diaminobenzidine tetrahydrocholoride (DAB) as a chromogen. Finally, the sections were counterstained with hematoxylin.

Immunohistochemical analysis. To assess p32 expression, we evaluated normal prostatic epithelium and carcinoma cells. In addition, an Allred score, which is a semi-quantitative system that takes into consideration the proportion of positive cells (scored on a scale of 0–5) and staining intensity (scored on a scale of 0–3), was determined for each case. The proportion and intensity were then summed to produce total scores of 0 or 2 through 8. A score of 0 was regarded as negative while weak was 2, moderate was 3–6 and strong was 7–8, as previously described.[19] Three people including a pathologist analyzed the expression independently and we used an average score of the intensity levels.

Statistical analysis. The statistical analyses were performed using JMP version 7.0.1. (SAS Institute Inc., Cary, NC, USA). We used the Chi-squared test for statistical analysis of the correlations between immunohistochemical p32 expression and clinicopathological parameters. Disease-free survival was taken as the period between surgery and the date of the last follow up or PSA recurrence by disease (n = 128). Survival curves were calculated by the Kaplan–Meier method, and the significance was analyzed by log-rank test. The Cox proportional hazards model was used for multivariate survival analysis, in which we estimated the hazard ratio. Two-sided $P < 0.05$ was considered statistically significant.

Cell culture. The cells used were the human prostate cancer cell lines LNCaP, PC3, Du145, 22Rv1 and primary prostate epithelial cells, RWPE-1. All cell lines were obtained from the American Type Culture Collection (ATCC). PC3, Du145, 22Rvl and LNCaP cells were grown in RPMI-1640 medium (Invitrogen) containing 5% fetal bovine serum (FBS). Normal epithelial RWPE-1 cells were grown in keratinocyte-SFM medium (Invitrogen) containing 5 ng/mL epidermal growth factor and 50 μg/mL bovine pituitary extract. All cells were cultured in a humidified incubator with 5% CO_2 and 95% air at 37°C. Charcoal-stripped FBS was used for assays of proliferation and p32 expression on the prostate cancer cell line.

Immunoblot analysis. Cells were lysed with Lysis buffer (50 mM Tris–HCl, pH7.5, 1 mM EDTA, 150 mM NaCl and 0.5% NP-40) and subjected to immunoblot analysis as described. Proteins were separated by SDS–PAGE and immunoblotted with the indicated specific antibodies. The signals were visualized with horseradish peroxidase-labelled anti-rabbit immunoglobulin G and an ECL reagent (GE Healthcare, Uppsala, Sweden). The chemiluminescence was recorded and quantified with a chilled charge-coupled device camera, LAS1000plus (Fuji Photo Film, Tokyo, Japan). Cell fractionation and intracellular localization of p32 were performed as previously described.[27]

Immunofluorescent imaging of prostate cancer cells. Human PC3, LNCaP RWPE-1 cells were incubated in the presence of 100 nM MitoTracker Red for 20 min. The cells were fixed, permealized and stained with 250-fold diluted anti-p32 antibody as previously described.[27]

Knockdown analysis using siRNA. The 25 bp double-stranded RNA targeting p32 was generated (Stealth Select RNAi; Invitrogen): 5′-AUAAUGACAGUCCAACACAAGGGCC-3′ and 5′-GGCCCUUGUGUUGGACUGUCAUUAU-3′. The siRNA transfection was performed according to the manufacturer's instructions (Invitrogen). The cells were seeded in six-well plates and assayed for the indicated time of western blotting and FACS analysis.

Cell proliferation assay. To determine cell proliferation, RWPE-1 and PC3 cells transfected with control- or p32-siRNA were seeded in 24-well plates at a density of 2×10^4 cells per

doi: 10.1111/j.1349-7006.2010.01828.x

well. After 24 h, one set of cells was trypsinized, resuspended in PBS and counted by a cell counter (Beckman Coulter Inc., Brea, CA, USA). The cells were counted in a similar way every 24 h, up to 120 h.

Cell cycle analysis. The cell cycle of RWPE-1 and PC3 cells were analyzed by flow cytometry with FACS caliber (Becton Dickinson, Franklin Lakes, NJ, USA). Cells were trypsinized and collected by centrifugation, washed and re-suspended in 0.1% BSA + PBS, and fixed in 70% ethanol at a density of 1×10^6 cells/mL. After the addition of 1000 units RNase A and 15 min incubation at room temperature, the cells were stained with 10 μL propidium iodide for 1 h. The cell cycle distribution was analyzed using the FlowJo software.

Results

Overexpression of p32 protein in prostate tumor tissues. Normal prostate tissue in the vicinity of prostate carcinoma was evaluated by immunohistochemistry for all 148 cases. p32 expression was mainly localized to the cytoplasm in epithelial cells and strong staining was observed in the cytoplasm of basal cells in normal glands (Fig. 1A). Luminal epithelial cells of normal prostate glands showed an homogenous moderate positivity. In tumor cells, p32 expression was strong and observed in the cytoplasm, but not in the plasma membrane (Fig. 1B–E). Increased intensity of homogeneous p32 expression was noted throughout the epithelium in high-grade prostate cancer. p32 expression of high-grade carcinoma was very strong, especially in poorly differentiated adenocarcinoma (Fig. 1D). Expression of p32 in normal prostatic epithelial cells was weak compared with that in the adjacent high-grade carcinoma cells (Fig. 1F). A total of 23/148 patients' carcinoma tissue showed strong expression of p32 also in the nucleus (Fig. 1G, arrows). Nuclear p32 expression was much less than the cytoplasm. Strong p32 expression was observed in mucinus adenocarcinoma in two samples (Fig. 1H).

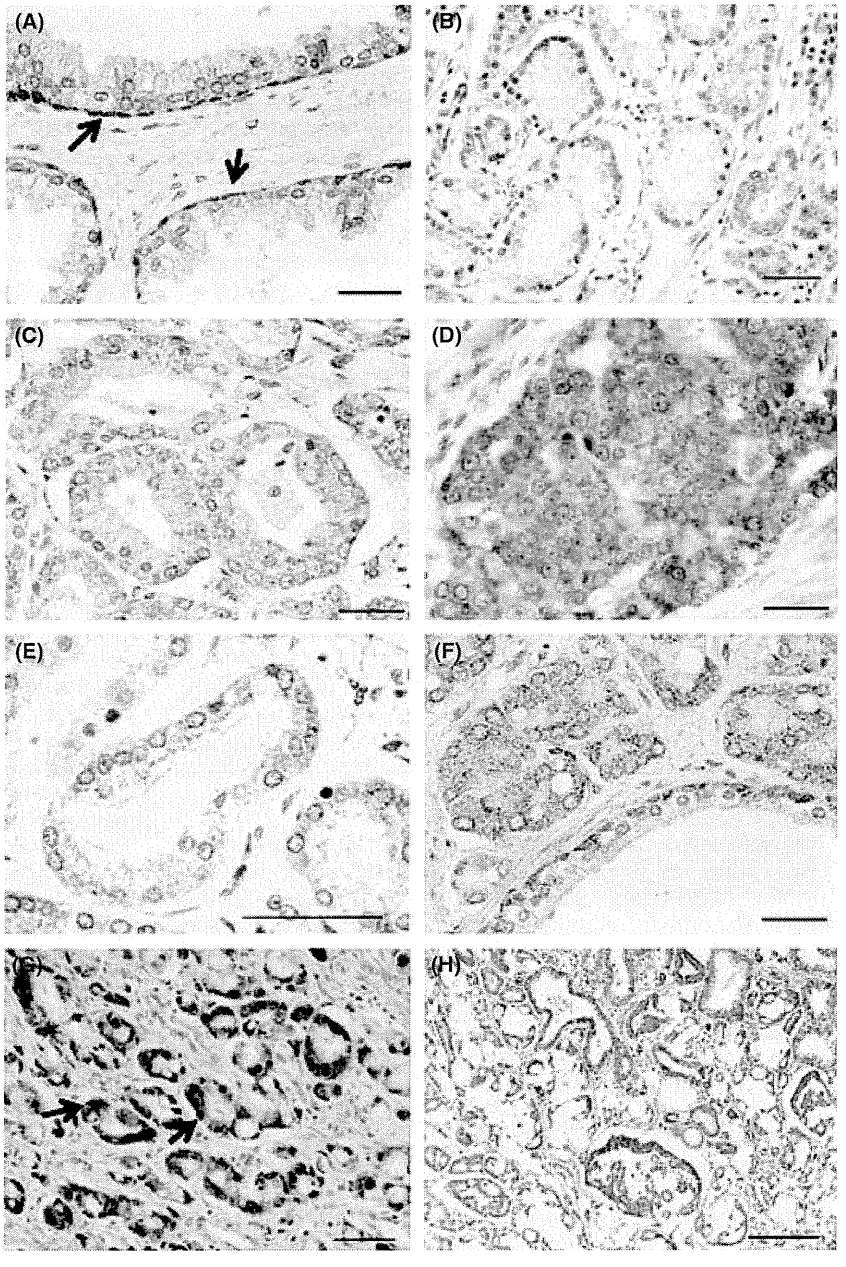

Fig. 1. Immunohistochemistry examination of the expression of p32. (A) A benign gland tissue. Weak p32 staining was evident in the cytoplasm of luminal epithelial cells of normal prostate glands, whereas the majority of basal epithelial cells revealed moderate or strong p32 positivity (arrows). (B) Weak p32 staining and (C) moderate p32 staining in a low-grade malignant tumor. (D) Strong p32 staining in a high-grade prostate cancer. (E) Moderate p32 expression in the cytoplasm with high magnification. (F) Normal prostate glands and adjacent high grade prostate carcinoma. (G) High-grade prostate carcinoma with nuclear staining of p32 (arrows). (H) Mucinus adenocarcinoma. Scale bar, 50 μm.

Correlations of p32 expression with clinicopathological factors and survival. We have summarized the correlations between p32 expression and the clinicopathological parameters in Table 1. p32 expression was significantly increased in higher Gleason score compared with lower Gleason score cancer ($P < 0.001$) and p32 expression was significantly increased in pT3 or more advanced cancer compared with pT2 cancer ($P = 0.01$). We also observed that p32 expression was increased in extraprostatic extension (EPE) positive compared with EPE negative (Supporting Information Table S2). A statistically strong significance was also observed between p32 expression and PSA relapse ($P < 0.001$). However, there was no significant association between p32 expression and patient's age, preoperative PSA, surgical margin or invasion (Table 1).

We observed strong expression in the nuclei of 23/148 patients' carcinoma tissue (Fig. 1G). We investigated the correlations between p32 nuclear expression and the clinicopathological parameters in Table 2. A statistically strong significance was observed between p32 nuclear expression and p32 cytoplasmic staining ($P < 0.01$). p32 nuclear expression was significantly increased in higher Gleason score ($P = 0.03$), pathological stage ($P = 0.02$) and preoperative PSA ($P = 0.01$) (Table 2).

Multivariate survival analysis of localized prostate carcinomas. The PSA recurrence-free survival rate was used as an end-point. Kaplan–Meier survival curve analyses of 102 prostate cancer tumors with clinical follow-up information showed that patients with high p32 expression in their tumors had a significantly reduced PSA recurrence-free survival rate compared with patients who had low p32 expression (log-rank test, $P = 0.0001$) (Fig. 2).

Next, we performed the Cox regression multivariate analysis with parameters including age, high p32 expression, Gleason score, high PSA and local metastasis. Table 3 summarizes the results of PSA recurrence-free survival analyzed by univariate and multivariate analysis. The Cox proportional hazards model revealed that strong p32 expression (4.10: hazard ratio [HR], 95% confidence interval [CI], 1.39–12.07; $P = 0.01$) and high PSA level (4.56: HR, 95% CI, 1.86–11.20; $P = 0.001$) were independent prognostic factors. The higher Gleason score (≥8) (3.22: HR, 95% CI, 0.87–11.89; $P = 0.08$) was not a significantly independent prognostic factor. Thus, high p32 expression consistently showed a strong and independent prognostic effect on clinical recurrence.

Table 1. Relationship between the expression of p32 and various clinicopathological characteristics

Variable	p32 expression			
	n (%)	Weak~Mod	Strong	*P*-value
Age (years)				
<70	99 (66.9)	57 (38.5)	42 (28.4)	0.45
≥70	49 (33.1)	25 (16.9)	24 (16.2)	
Gleason score				
≤6	39 (26.4)	31 (21.0)	8 (5.4)	<0.001†
7	97 (65.5)	49 (33.1)	48 (32.4)	
≥8	12 (8.1)	2 (1.4)	10 (6.8)	
Preoperative PSA (ng/mL)				
<10	89 (62.2)	50 (35.0)	39 (27.3)	0.88
≥10	54 (37.8)	31 (21.7)	23 (16.1)	
Pathological stage				
pT2	101 (68.2)	63 (42.6)	38 (25.7)	0.01†
pT3~T4	47 (31.8)	19 (12.8)	28 (18.9)	
Surgical margin				
Negative	81 (54.7)	49 (33.1)	32 (21.6)	0.17
Positive	67 (45.3)	33 (22.3)	34 (23.0)	
Invasion				
Negative	136 (91.9)	77 (52.0)	59 (39.9)	0.31
Positive	12 (8.1)	5 (3.4)	7 (4.7)	
Relapse				
(–)	115 (81.6)	72 (51.1)	43 (30.5)	<0.001†
(+)	26 (18.4)	5 (3.6)	21 (14.9)	

†Statistically significant (Chi-squared test). PSA, prostate-specific antigen.

Table 2. Relationship between the nuclear expression of p32 and various clinicopathological characteristics

Variable	p32 expression of nucleus			
	n (%)	–	+	*P*-value
Age (years)				
<70	99 (66.9)	84 (56.8)	15 (10.1)	0.85
≥70	49 (33.1)	41 (27.7)	8 (5.4)	
p32 expression				
Weak~moderate	82 (55.4)	80 (54.1)	2 (1.4)	<0.01†
Strong	66 (44.6)	45 (30.4)	21 (14.2)	
Preoperative PSA (ng/mL)				
<10.0	89 (62.2)	80 (55.9)	9 (6.3)	0.01†
≥10.0	54 (37.8)	40 (28.0)	14 (9.8)	
Gleason score				
≤6	39 (26.4)	38 (25.7)	1 (0.7)	0.03†
7	97 (65.5)	77 (52.3)	20 (13.5)	
≥8	12 (8.1)	10 (6.8)	2 (1.4)	
Pathological stage				
pT2	101 (68.2)	90 (60.8)	11 (7.4)	0.02†
pT3-4	47 (31.8)	35 (23.7)	12 (8.1)	

†Statistically significant (Chi-squared test). PSA, prostate-specific antigen.

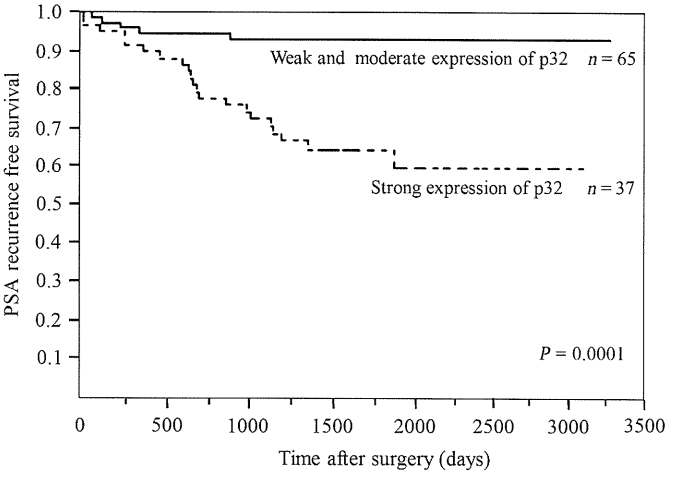

Fig. 2. Disease-free survival curves of patients in high and low p32 expression groups. Disease-free survival was analyzed using the Kaplan–Meier method for high and low p32 expression in localized prostate cancer with clinical recurrence. *P*-values were obtained by a log-rank test ($P = 0.0001$).

p32 expression of human prostate cancer cell line. To find the molecular mechanism of p32 in prostate tumor progression, we first investigated the expression of p32 in human prostate cancer cell lines and noncancerous cell line RWPE-1. High p32 expression was seen in all prostate cancer cell lines examined (PC3, 22Rv1, LNCaP and Du145) compared with the noncancerous cell line RWPE-1 (Fig. 3A). There was no difference in the β-actin and TFAM (mitochondrial DNA nucleoid protein) expressions among the cell lines (Fig. 3A).

p32 localized in mitochondria. Because we observed strong expression of p32 in the nuclei of carcinoma tissue, we investigated

doi: 10.1111/j.1349-7006.2010.01828.x